Physics – Uspekhi **54** (1) 9 – 28 (2011)

REVIEWS OF TOPICAL PROBLEMS

PACS numbers: 41.75.Jv, **42.55. – f**, 42.62.Be, 42.65.Yj, 52.38.Kd, 52.38.Ph

CELEBRATING 50 YEARS OF THE LASER

Horizons of petawatt laser technology

A V Korzhimanov, A A Gonoskov, E A Khazanov, A M Sergeev

DOI: 10.3367/UFNe.0181.201101b.0009

Contents

Abstract. Recent advances in the development of superpower lasers are reviewed. A number of possibilities that the newly available petawatt-power level lasers open up in the physics of extreme light fields are discussed.

1. Introduction

The tremendous upgrowth of laser technologies after the invention of the chirped (frequency-modulated) pulse amplification method in 1985 [1, 2] has resulted in the creation of laser systems capable of generating radiation in excess of 1 PW [3–5]. The quality of the beams thus produced has allowed focusing them onto a spot a few wavelengths in diameter and has ensured radiation intensity of the order of 10^{22} W cm^{-2} [6, 7]. Investigations of the mechanisms of interaction between such intense radiation and matter is a fundamental problem facing modern physics; these mechanisms are being extensively studied both theoretically and experimentally by many research groups [8, 9].

A V Korzhimanov, A A Gonoskov, E A Khazanov, A M Sergeev
Institute of Applied Physics, Russian Academy of Sciences,
ul. Ul'yanova 46, 603950 Nizhny Novgorod, Russian Federation
Tel. (7-831) 416 48 48, (7-831) 236 57 36. Fax (7-831) 236 37 92
E-mail: kav@ufp.appl.sci-nnov.ru, khazanov@appl.sci-nnov.ru, ams@ufp.appl.sci-nnov.ru

Received 15 November 2010
Uspekhi Fizicheskikh Nauk **181** (1) 9 – 32 (2011)
DOI: 10.3367/UFNr.0181.201101b.0009
Translated by Yu V Morozov; edited by A M Semikhatov

The methods for laser pulse compression, such as the mode-locking technique [10], developed since the demonstration of the first laser 50 years ago, permitted exponentially increasing the intensities; the level of 10^{14} W cm^{-2} was surpassed by the late 1960s. This seemed to be a natural limit for ordinary laser media because attempts to obtain higher intensities resulted in radiation self-focusing, optical breakdown, and disintegration of the materials used.

The invention of the chirped pulse amplification (CPA) method allowed overcoming these difficulties. The idea behind CPA (see Fig. 1) consists in passing the starting laser pulse through a stretcher, an optical dispersion system in which the pulse undergoes strong linear frequency modulation (so-called chirp modulation). As a result, the originally short pulse stretched out ten thousand-fold in time and space due to the separation of its spectral components. The intensity of such a stretched (chirped) pulse is much lower than that of the initial pulse. Thereafter, the pulse is amplified in the usual way and passed through a second dispersion system (called the compressor), an inverse of the first one. A pair of diffraction gratings is typically used as the stretcher and the compressor properly positioned and oriented with respect to the optical path of the laser pulse. An advantage of this scenario is that only the stretched pulse is amplified in the laser medium, which prevents a breakdown. At the same time, the sole region where the high-intensity pulse interacts with matter is the surface of the last diffraction grating that compresses the pulse, whose damage threshold is much higher than the level causing the breakdown in the core of optical materials. The CPA method has been used in the past 20 years to increase

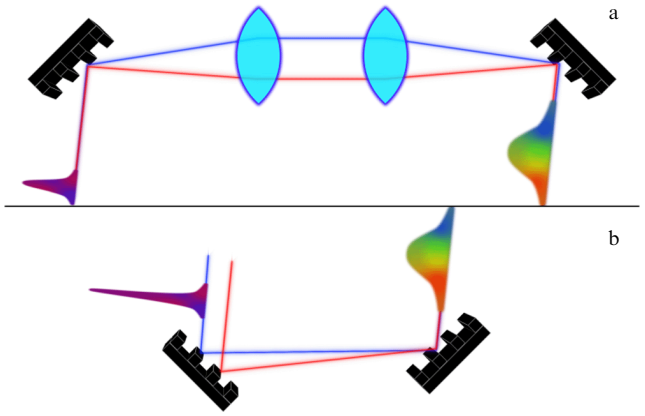

Figure 1. Schematic diagram of the CPA technology. (a) The principle of stretcher operation: a short pulse passes through a dispersion system with different paths for different wavelengths. As a result, the output pulse becomes stretched out in space and chirped. (b) The principle of operation of the compressor (the inverted stretcher): the output pulse becomes compressed again.

laser radiation intensity by 5–6 orders of magnitude up to 10^{22} W cm^{-2} [6, 7].

The most efficient laser medium in such systems is sapphire crystals doped with titanium ions (Ti^{3+}:Al_2O_3 or Ti:Sa). The broad-band amplification (up to 3000 cm^{-1}) in such crystals produced the record-breaking intensities owing to the very short duration of radiation (tens of femtoseconds) at relatively low pulse energies (tens of Joules). By contrast, in CPA devices with the amplification in Nd:glass, petawatt power is achieved in longer ($\sim$ 1 ps) pulses with much higher energies (around 1 kJ).

A new method for the generation of superpower pulses was being developed in parallel to CPA based on parametric light amplification in nonlinear optical crystals (optical parametric pulse amplification, OPCPA). Piskarskas and coworkers [11] were the first to propose the use of parametric amplification, instead of the ordinary laser one, to generate superpower pulses in 1986. This idea was later realized by several experimental groups [12–16]. An advantage of OPCPA is the unprecedentedly high amplification factor of chirped pulses: up to 3–4 orders of magnitude per pass in terms of energy. Another benefit is the well-developed technology for the growth of wide-aperture potassium dihydrophosphate (DKDP) crystals, which allows increasing the energy of the pulses being generated by scaling the amplification cascades [17, 18]. At present, three classes of amplifiers are available based on Ti:Sa crystals and Nd:glass for CPA and on deuterated potassium dihydrophosphate (DKDP) crystals for OPCPA. Their power level is approximately the same (1 PW).

The development of laser technologies for the generation of terawatt and petawatt optical pulses gave an impetus to the research of the physics of interactions between superstrong optical fields and matter [8]. These interactions are typically nonlinear because of rapid changes in the matter state and excitation of various dynamic processes. We note that the electric field of a laser pulse becomes comparable with the characteristic value of the intra-atomic field when the radiation intensity reaches the 10^{15} – 10^{16} W cm^{-2} level. This leads to rapid (at times smaller than the optical vibration period) ionization of matter and plasma formation. This way, the physics of superstrong fields studies the interactions between laser radiation and hot nonequilibrium plasma. One more essential issue is that the electron motion in a 1 μm wave field of the order of 10^{18} W cm^{-2} becomes relativistic because the electron oscillation energy exceeds their rest energy. Studies of the effects emerging from interactions in such a regime gave rise to a new branch of physics called relativistic optics [8] or the physics of relativistic laser plasma. Two main effects should be distinguished that play key roles in the interaction dynamics. First, the Lorentz increase in the effective electron mass occurs, leading to an effective decrease in the plasma frequency, which in turn affects plasma optical properties and causes the so-called relativistic nonlinearity responsible for the effects such as relativistic self-focusing [19, 20] and relativistic self-induced transparency [21, 22]. Second, the role of the magnetic constituent of the Lorentz force significantly increases as it becomes comparable to the electric one. As a consequence, the role of the high-frequency ponderomotive force acting on an electron increases [23]. The ponderomotive effects are responsible for the phenomena such as excitation of wakefield plasma waves in transparent plasma [24–26] and generation of higher harmonics on the surface of a solid target [27].

The problem of interaction between superpower laser radiation and matter is interesting not only from the theoretical but also from the practical standpoint, taking into consideration that it is a key problem for many important applications. These include the generation of beams of charged particles [28, 29] (both electrons [30, 31] and ions), neutron beams [32–34], high harmonics in the X-ray range [27, 35], and noncollisional heating of the plasma to relativistic temperatures [36-38]. Also, high-power laser pulses are important for research on inertial confinement fusion [39, 40] and the solution of the related problem of fast ignition [41, 42].

2. Brief review of large-scale international and national superpower laser development and application projects

Laser centers all over the world house about 20 devices with the peak power over 100 TW and the pulse duration below 1 ps. At least 10 more facilities with similar characteristics are under construction or being upgraded. Moreover, there are a few major systems for laser-induced thermonuclear fusion, viz. NIF (National Ignition Facility, USA), LMJ/PETAL (Laser MegaJoule/PETawatt Aquitaine Laser, France), and the HiPER project (High Power Laser Energy Research, UK) in which nanosecond laser pulses are used (or planned to be used) from tens of radiation channels with the total power close to the aforementioned one. Moreover, picosecond multi-petawatt laser channels for fast ignition are being designed. The table below lists the main national laser projects and operating facilities, along with their characteristics.

Of special interest are promising projects that are either at the preparatory design phase or at the onset of implementation intended to reach multipetawatt powers. They include two European infrastructure megaprojects, ELI (Extreme Light Infrastructure) and HiPER; Vulcan-10PW being implemented at Rutherford and Appleton Laboratories (RAL, UK); ILE (Ile-Apollon, Institut de la Lumiere Extreme, France); and PEARL-10 (PEtawatt pARametric Laser, Institute of Applied Physics, Russian Academy of Sciences).

Table. Operating facilities with a peak power $\geqslant 100$ TW at pulse duration $\leqslant 1$ ps.

Country System name Research center	Laser type	Peak power	Pulse energy, J	Minimum duration, fs	Max. intensity, W cm^{-2}	Repetition rate	Main lines of research
Russia							
Femta-Luch Russian Federal Nuclear Center All-Russian Research Institute of Experimental Physics (RFNC-VNIIEF)	DKDP	1 PW	70	70		Several times daily	Physics of laser fusion (LF), extreme states of matter, particle acceleration
PEARL Institute of Applied Physics (IAP RAS)	DKDP	560 TW	24	43		Several times daily	Electron acceleration, biomedical applications
USA							
NIF Lawrence Livermore National Laboratory (LLNL)	Nd:Glass		1.8×10^6	3×10^3		Several times daily	Laser fusion
Callisto LLNL	Ti:Sa	300 TW	18	60			Electron acceleration
Trident Los Alamos National Laboratory (LANL)	Nd:Glass	200 TW	100	500			Ion acceleration, laboratory astrophysics
OMEGA EP Laboratory for Laser Energetics, University of Rochester (LLE)	Nd:Glass	1 PW			10^{20}		New ignition systems for LF
Hercules Center for Ultrafast Optical Science (CUOS), University of Michigan	Ti:Sa	300 TW	17	50	2×10^{22}	0.1 Hz	Relativistic laser plasma, particle acceleration, X-ray generation
Texas Petawatt University of Texas (UT)	Nd:Glass	1.1 PW	186	165		Several times per hour	Particle acceleration, biomedical applications
Great Britain							
Vulcan Rutherford and Appleton Laboratories (RAL)	Nd:Glass	1 PW	500	500	10^{21}	Several times per hour	LF physics, extreme states of matter, particle acceleration, laboratory astrophysics
Astra Gemini RAL	Ti:Sa	2×0.5 PW	2×20	40	10^{22}	1/20 Hz	Particle acceleration, coherent X-ray sources, laboratory astropysics
France							
Laboratoire pour l'Utilisation des Lasers Intenses (LULI), École Polytechniqe	Nd:Glass	100 TW	30	300		Once every 20 min	Laser–matter interaction
Laboratoire d'Optique Appliquée (LOA)	Ti:Sa	100 TW	2.5	25		10 Hz	Particle acceleration
Germany							
ATLAS Max-Planck Institut für Quantenoptik (MPQ)	Ti:Sa	100 TW	2	25		5 Hz	Particle acceleration
PHELIX Gesellschaft für Schwerionenforschung (GSI)	Nd:Glass	1 PW	500	500			Interaction of laser radiation and heavy ion beams
Universität Dusseldorf	Ti:Sa	100 TW	2.5	25			Relativistic laser physics

Table (continued)

Country System name Research center	Laser type	Peak power	Pulse energy, J	Minimum duration, fs	Max. intensity, W cm^{-2}	Repetition rate	Main lines of research
Japan							
Institute of Laser Technologies (ILE), University of Osaka	Nd:Glass	1 PW	500	500	10^{20}	3 – 4 times daily	LF, high energy density physics
Advanced Proton Research Center (APRC), Japan Atomic Energy Agency (JAEA)	Ti:Sa	850 TW		33		10 Hz	Relativistic optics
Canada							
ALLS Institut National de la Recherche Scientifique (INRS)	Ti:Sa	200 TW	5	25		10 Hz	Interaction with matter in the X-ray to IR range
Korea							
Institute of Science and Technology, Gwangju (GIST)	Ti:Sa	100 TW 1 PW	3 30	30 30		10 Hz 0.1 Hz	Relativistic Thomson scattering, generation of hard X-rays, electron acceleration
China							
Shanghai Institute of Optics and Fine Mechanics (SIOM)	Ti:Sa	890 TW		29		10 Hz	Relativistic laser plasma, particle acceleration, X-ray generation

2.1 European ELI megaproject

The ELI project is an integral part of the unique research infrastructure accessible to researchers studying laser–matter interactions at a maximally attainable power level and to developers of relevant applications. The four main types of applications are the physics of the vacuum in extremely strong light fields, attosecond physics, the creation of secondary sources of accelerated charged particles and hard photons, and nuclear processes in superstrong laser fields.

The most promising component of ELI is a laser generating pulses with the peak power 0.2 exawatt (0.2×10^{18} W). Such power will be achieved by concentrating a relatively small energy ($\sim$3–4 J) for very short time intervals (around 15 fs). It is expected that despite the small energy of ELI compared with that of mega-Joule facilities for LTF, its peak power will be hundreds of times higher than in the currently existing most powerful lasers due to the ultrashort pulse duration. In addition to the exawatt laser, three more unique laser facilities with the peak power 10 to 20 PW will be built.

The ELI laser facilities are expected to significantly promote the development of science and technology in the aforementioned research fields and to create formerly undreamt of conditions for studies on plasma physics, astrophysics, and nuclear and high-energy physics. These facilities will provide a basis for the creation of unique sources of hard photons and high-energy charged particles with the formerly unattainable brightness and spatial concentration of electromagnetic energy on a nanometer spatial and attosecond temporal scale. The use of ELI-generated ultrabright proton beams and X-rays in proton/ion therapy, phase-contrast imaging, and radiography of isolated biological molecules and nanoobjects will promote further progress in the diagnostics and treatment of malignancies and will find application in structural biology. Ultrabright attosecond X-ray beams, in turn, may be used to obtain four-dimensional images with subatomic resolution in order to detect changes in the microscopic structure of matter with picometer spatial and attosecond temporal resolution.

The ELI laser systems will be based on the technologies currently developed in three leading centers: Institut de la Lumière Extrême, Max-Planck Institut für Quantenoptik (MPQ) (Germany), and Rutherford and Appleton Laboratories (RAL). The 10 PW ILE Apollon laser is being designed in the framework of the ILE project based on the CPA technology with the final amplification cascade using a Ti:Sa crystal 20 cm in diameter. MPQ developed the basic technology for the amplification of ultrashort (5 fs) pulses by OPCPA technology using nonlinear optical BBO crystals. The same technology is used at RAL to build up the wide-aperture DKDP-based Vulcan-10PW laser.

The preparatory stage of the project (2008–2011) is currently underway, supported by the 7th European Union framework program of infrastructure megaprojects. The overall cost of the project to be covered by the EU infrastructure for 5–6 years is estimated at 740 mln euros, with over 600 researchers directly involved in its implementation. The part of ELI will be realized in the Czech Republic (basic physical processes in superstrong electromagnetic fields), Hungary (atto- and zeptosecond beam studies), and Romania (photonuclear processes).

2.2 International HiPER project

The aim of the HiPER project is to build the first demonstration reactor for inertial confinement fusion, an analog of the international thermonuclear experimental reactor (ITER) for controlled magnetic confinement fusion. The preparatory stage of the project is to be completed in 2011; its further development into the demonstration phase will depend on the immediate results to be obtained at the NIF facility, USA (see the table). The startup of all NIF laser channels in 2009 allowed initiating experimental compression of thermonuclear targets; the fast ignition of nuclear fusion in the indirect

irradiation regime with the energy output coefficient 10–30 is expected to be demonstrated within the next 1–2 years. The experimental proof of the 'existence theorem' half a century after it was formulated will finally allow the practical application of nuclear fusion for energy production. The, HiPER project may become the first international laser fusion reactor.

Given the success of the NIF facility, the HiPER project will enter the demonstration phase in 2011–2012; during the next decade, a laser system for firing up a fusion reaction with the repetition rate 5–10 Hz will be built, along with a laser target fabric, a chamber for radiation–target interaction, and an outer shell for the conversion of thermonuclear energy into heat. The laser facility will have about 50 channels for quasihomogeneous target compression with the mean radiation power about 100 kW, the pulse energy 10 kJ per channel, the pulse repetition rate 5–10 Hz, and the pulse duration of a few nanoseconds. Separate channels with multi-petawatt power and picosecond pulses are needed to start up a reaction in the fast ignition or shock wave regime.

The operational phase of the project is scheduled for the 2020s, when HiPER must become a reliable integral system with the well-tested operating technologies meeting the future energy production standards and reliability criteria. It will be the prototype facility for building nuclear power plants all over the world.

It should be borne in mind that there is currently no system of laser, plasma, nuclear, thermoenergetic, or other technologies for the detailed practical designing of such a facility. This opens up a wide range of opportunities for international cooperation at the demonstrator phase of the HiPER project and involvement of Russian research centers in its implementation. Russian researchers could contribute to the entire spectrum of the above technologies, especially laser engineering and the physics of interaction of high-power laser pulses with matter.

2.3 Vulcan-10PW laser facility

The aim of the Vulcan-10PW laser project (UK) is to create a source of 30 fs laser pulses with the energy 300 J, the intensity up to 10^{23} W cm^{-2}, and the repetition rate of two pulses per hour using the OPCPA technique. For pumping, the Vulcan-10PW facility will use kilo-Joule pulses generated on amplification cascades of the Vulcan laser, the two final OPCPA cascades to be based on wide-aperture (40×40 cm) DKDP crystals. The building of the 10 PW laser is scheduled to begin in the second half of 2010, to be completed in 2013; in this period, the Vulcan machine will be inaccessible to experimenters.

A similar project (PEARL-10) is being implemented in Russia based at the Institute of Applied Physics, Russian Academy of Sciences. It employs an original OPCPA technology on the wide-aperture DKDP crystals with which the petawatt PEARL and Femta-Luch (Ray) lasers have been built. The Russian researchers are thus ahead of their RAL colleagues as regards this technology (with terawatt power level achieved); in fact, their advances gave the impetus for the initiation of the Vulcan-10PW project.

2.4 ILE Apollon laser facility

The ILE Apollon project (Institut de la Lumière Extrême, France) has the objective of creating a laser with the peak power 10 PW, maximum intensity 10^{24} W cm^{-2}, pulse energy 150 J, and duration 15 fs at the repetition rate of 1 per min. The final amplification cascades will be realized using active Ti:Sa crystals 20 cm in diameter. Crystals of this size and optical quality are currently unavailable, but a few manufacturers are trying to grow them. Another important technology to be developed is the creation of pump lasers with kilo-Joule energies operating at the repetition rate of 1 shot every min. A serious problem is the absence of adaptive mirrors to correct the wave front for focusing high-energy pulses onto a spot roughly 1 μm in diameter and thereby to reach the desired intensity. Other technical difficulties are to be overcome to realize the project.

We note that the ILE Apollon project is supposed to contribute to developments within the framework of ILE. First, the Apollon laser system will provide a basis for the Czech and Romanian ELI facilities. Second, Institut de la Lumière Extrême will be the leading developer of the fourth ELI facility for studying properties of the vacuum in superstrong fields in France after 2012, and Apollon may serve as the forerunner of a separate channel of the exawatt laser.

2.5 PEARL-10 laser system

The PEARL-10 project is being implemented at the Institute of Applied Physics, Russian Academy of Sciences, where a 0.56 PW laser generating 45 fs pulses with the energy 25 J was launched in 2007. Today, it is one of the world's most powerful lasers. PEARL-10 employs parametric amplification in a 10×10 cm aperture DKDP crystal obtained at the institute by the original rapid directional growth technology. At present, this technology is used to grow crystals with the aperture 40×40 cm, which opens up unprecedented opportunities for the further development of OPCPA. The PEARL-10 project based on the results of previous studies has the objective of creating a source of 20 fs laser pulses with the energy in excess of 200 J, maximum intensity over 10^{23} W cm^{-2}, and repetition rate of 1 shot per min. This system will be operated in the OPCPA mode using DKDP crystals with the final cascade aperture 20×20 cm.

The program of research using the PEARL-10 facility includes:

- creating sources of bright ultrashort coherent and incoherent radiation in hard X-ray and gamma ranges based on synchrotron emission of ultrarelativistic charged particles in superstrong laser fields; the use of these sources to diagnose processes and structures with pm spatial and fs temporal resolution;
- building compact laser accelerators of ions with the energy 10–1000 MeV and the development of their applications, including those for radiotherapy; creation of 1–10 GeV laser-driven electron accelerators; high-energy physics research to provide a basis for prototype accelerators in the framework of the ILC (International Linear Collider) project;
- developing and studying extreme states of matter arising under the effect of laser fields of ultrarelativistic intensity; laboratory-based simulation of astrophysical and early cosmological phenomena; investigation of nonlinear properties of the vacuum in strong laser fields, generation of electron–positron pairs and particle showers.

To summarize, over the next few years, several countries may be expected to create sources of laser pulses with the peak power up to 10 PW and intensity 10^{23} W cm^{-2}. In this context, it is interesting to discuss new possibilities to be provided by these facilities for the physics of extreme light–matter interactions. In Sections 3–5, such a discussion focuses on the problems of laser particle acceleration and develop-

ment of new ultrabright and ultrashort radiation sources emitting radiation in the hard X-ray and gamma ranges.

3. Laser-driven electron acceleration: the concept, the state of the art, and new ideas

3.1 Acceleration by a focused laser field

Electromagnetic fields of the currently available laser pulses greatly surpass the limiting fields (not higher than 100 MW m^{-1}) in linear accelerators, where the restrictions are first and foremost due to wall breakdown. However, these fields oscillate in time and their vectors are oriented across the propagation direction, which accounts for the low efficiency of electron acceleration under their influence. A longitudinal electric field can be high in the case of fine focusing, but the phase velocity along the propagation axis is greater than the speed of light, which makes electrons rapidly leave the field acceleration phase. Given an optimal choice of the focusing angle, the maximum addition to the electron energy is defined by the expression $dW\,[\mathrm{MeV}] = 31(P\,[\mathrm{TW}])^{1/2}$ [43], where a first-order Laguerre–Gauss mode is used. A 30 keV modulation on an electron beam with the energy 30 MeV was observed experimentally in the interaction with a pulse having the energy 0.5 mJ and duration 4 ps in a vacuum region semibounded by an 8 mm gold-coated kapton film placed in the focus [44]. An alternative approach is to introduce a background gas into the interaction region for reducing the phase speed to below the speed of light, and thereby to lengthen the electron path in the acceleration phase [45]. The use of the gas may, in principle, facilitate solution of the laser beam diffraction divergence problem owing to self-channeling (self-focusing) [46]. But the use of a gas is seriously limited by its ionization, which begins at relatively low intensities (of the order of 10^{14} W cm^{-2}). A 3.7 MeV modulation was demonstrated in an experiment using an electron beam with the energy 40 MeV and a 500 MW CO_2-laser pulse propagating within the 12 cm gas-filled region [45]. Generally speaking, the most essential limitation inherent in all concepts of direct laser-driven electron acceleration is attributable to the very short radiation wavelength (typically of the order of 1 μm).

3.2 Acceleration in a plasma wave

The use of plasma permits obviating most difficulties related to direct electron acceleration, such as diffraction divergence of a laser beam, gas ionization in the interaction region, and rapid escape of electrons from the acceleration phase. The idea of charged particle acceleration by powerful laser pulses during the interaction with the plasma, first suggested in 1979 [25], is as follows. A laser pulse propagating in a transparent plasma has a ponderomotive effect on electrons along the direction of its motion and thereby induces plasma oscillations in the form of a wakefield plasma wave. The excited wave has a longitudinal electric field having both acceleration phases in which the electrons are accelerated parallel to the laser pulse, and deceleration phases in which they slow down. Because the acceleration zones move with the phase speed equal to the group velocity of the laser pulse in the plasma and close to the speed of light, the electrons present in the acceleration phase and propagating with a relativistic speed in the direction of the laser pulse remain in this phase for a rather long time and acquire a high energy. Such electrons are referred to as captured, and the energy gain is limited by the dephasing length, i.e., the distance covered by the captured electrons before they leave the wakefield wave acceleration phase. The main advantage of plasma-mediated acceleration is that the longitudinal electric field of the wakefield wave may be significantly higher than the accelerating field in a traditional linear accelerator; this allows decreasing its length by several orders of magnitude. The idea of laser-driven acceleration of charged particles aroused great interest because, in principle, it provides the possibility of having small laboratory accelerators with characteristics satisfying the requirements for a number of important applications for which much more expensive bulky accelerators are needed.

3.2.1 Acceleration in a linear regime. There are several concepts of wave excitation in the framework of the general idea of laser electron acceleration by a wakefield wave. The laser wakefield accelerator (LWFA) concept proposed in [25, 47, 48] consists in using an intense ($> 10^{17}$ W cm^{-2}) laser pulse shorter than the time for which light covers the distance equal to the plasma wavelength. However, such laser sources were unavailable until the advent of the CPA method, and wakefield waves were excited by the method of plasma beat wave acceleration (PBWA) [25, 49–53]. The idea behind PBWA is a three-wave excitation by two laser pulses whose frequency difference is equal to the plasma frequency [54–59]. The PBWA concept has the disadvantage of an increase in the plasma wave period with amplitudes and a sharp decrease in the excitation efficiency due to departure from the resonance conditions. These problems were resolved in the framework of the multipulse excitation concept, in which a plasma wave is excited by a sequence of short pulses following one another at a certain interval such that each subsequent pulse resonantly amplifies the wave excited by the previous one [60–64]. The pulse sequence necessary to excite a plasma wave may form under certain conditions during self-modulation of a single laser pulse. Accordingly, the concept of electron acceleration based on such a manner of plasma wave excitation is called the self-modulated plasma beat wave acceleration (SM-PBWA) technique [50, 65–78].

Certain experiments carried out between 1995 and 2004 demonstrated laser-driven electron acceleration up to 100 MeV with accelerating fields in excess of 100 GV m^{-1} and the total charge of the accelerated electrons higher than 1 nC [70, 71, 76, 79–82]. However, accelerated electron beams in these experiments showed an exponential distribution over energies, and the electrons mostly acquired energies below 10 MeV.

The expression for the ponderomotive force acting on plasma electrons during propagation of a laser pulse can be derived from plasma hydrodynamics equations in a linear approximation ($|a| = e\,|\mathbf{A}|/m_e c^2 \ll 1$) in the form $\mathbf{F}_p = -m_e c^2 \nabla(a^2/2)$, where $\mathbf{A}$ is the vector potential, m_e and e are the electron mass and charge, and c is the speed of light [83]. This force is sometimes referred to as the light pressure force. It follows from the above expression that plasma electrons are expelled by the ponderomotive force from the region containing an electromagnetic field. Generation of a wakefield wave by a laser pulse in the three-dimensional geometry and a linear regime was analytically considered in the framework of a hydrodynamic model [47, 48, 57]. Theoretical studies are restricted by the condition of a maximum plasma wave longitudinal field of the form $E \ll E_0$, where $E_0 = m_e c\omega_p/e$ is the vortex field in the nonrelativistic

treatment, $\omega_p = (4\pi e^2 N_e/m_e)^{1/2}$ is the plasma frequency, and N_e is the plasma electron concentration. The wakefield wave being excited creates not only an electric field along the propagation axis but also a radial electric field and a transverse vortex magnetic field as a natural consequence of the finiteness of the pulse transverse size. The structure of these fields is such that the trapped electrons are alternately accelerated and focused with respect to the axis. In this way, an electron beam whose Coulomb repulsion forces are compensated by wakefield wave fields may undergo continuous acceleration in the wave acceleration phase. A detailed theoretical study of the processes of wakefield wave generation and electron acceleration is reported in [84–86].

An important problem arising in the linear acceleration regime is the electron loading and trapping in the field acceleration phase. Its theoretical study based on the electron Hamiltonian in a reference frame moving with the phase speed revealed a minimal threshold value of the electron pulse necessary for its capture [87]. This value is determined by the parameters of the problem; specifically, it decreases as the plasma wave amplitude increases and the wave speed decreases [88]. Therefore, one of the trapping mechanisms is the self-capture after high-energy electron pulses in the temperature distribution 'tail' surpass the threshold value. Plasma instabilities and Raman light scattering play important roles by lowering the capture threshold [89–91]. The self-capture mechanism highly effectively operates in situations close to plasma wave breaking [70, 74, 92]. We note that electron trapping is restricted by previously captured electrons owing to the action of Coulomb repulsion forces. The trapped charge is normally smaller than 10 nC, has the Boltzmann distribution, and has a temperature of several MeV. One way to solve the electron injection problem is to inject a short electron beam from an external source in the proper phase. But the formation of electron beams of a desired duration in traditional accelerators is an extremely difficult task because plasma waves usually have a very small size ($\lambda_p \sim 30$ μm for $N_e \sim 10^{18}$ cm^{-3}). An alternative approach is to create conditions for trapping using another laser pulse [93–98]. The possibility of capture in head-on pulse collisions was demonstrated in experiment [99, 100]. One more electron capture method is based on the use of inhomogeneous plasma with the density gradient directed along the wakefield wave distribution [101–106]. This idea was realized experimentally in 2008 [107].

Thus far, electrons with an energy of the order of 1 GeV have been obtained in the linear acceleration regime [108, 109] using a 3 cm track of a discharge-produced low-density plasma. The difficulty was posed by diffraction divergence of the laser beam, which was compensated by propagation in a capillary waveguide.

3.2.2 Acceleration in a nonlinear regime. The amplitude of a plasma wave increases with the laser field amplitude until it becomes nonlinear [110–112]. As the field amplitude surpasses a certain threshold, the plasma wave breaks [21, 113, 114], and the so-called cavitation (bubble) regime sets in [115–117]. In this regime, a cavitation area totally devoid of electrons forms behind the laser pulse. Electrons either injected or spontaneously trapped in the cavitation region may remain there for a long time and may be accelerated to high energies. In this way, quasimonoenergetic electron beams are formed. It is in this regime that such beams are believed to have been obtained for the first time [118–120]. Electron acceleration has recently been investigated in the cavitation regime both theoretically and experimentally [121, 122].

In 2009, in-depth studies of this process allowed generating electron beams with energies 700–800 MeV in experiment. First, energies of the order of 800 MeV were achieved at the Astra Gemini facility in RAL [121], then electron beams with energies 720 ± 50 MeV were obtained with the Callisto laser at the Lawrence Livermore National Laboratory (LLNL), USA [123]. Similar parameters were used in both experiments: the radiation power at a 200 TW level and the maximum intensity around 2×10^{19} W cm^{-2}.

Callisto experiments appear to have been especially successful. The study of the dependence of acceleration efficiency on the gas density in a jet performed by the LLNL group revealed a threshold concentration of electrons (2.5×10^{18} cm^{-3}) necessary to trigger their self-capture in the acceleration cavity [124]. Numerical simulation showed that acceleration was hampered by the fact that the electron self-capture occurred much later than the accelerating structure formed. Another problem was the complex evolution of the cavitation structure during acceleration, accounting for electron capture in the second rather than the first cavity behind the laser pulse and lowering the efficiency of acceleration. This process was investigated in [125], where the generation of electron beams with energies of the order of 300 MeV by a 100 TW laser pulse is described. The researchers at LLNL overcame this problem by introducing readily ionizable carbon dioxide molecules (3%) into helium to facilitate electron acceleration. The experiment in [126] was performed with a 110 TW laser pulse 60 fs in duration. The beam width was 15 μm, which created the near-optimal conditions for bubble formation. The jet length was 1.3 cm and the plasma concentration $(1.3 \pm 0.1) \times 10^{18}$ cm^{-3}. The output electron beam energy amounted to 1.45 GeV (currently, the highest energy for laser acceleration systems).

3.2.3 Alternative scenarios. Electron acceleration occurs in other regimes besides those described in the preceding sections. Worthy of special mention is acceleration in a self-modulated wakefield plasma wave [127–129] and a variety of hybrid systems. A two-step scenario was proposed recently [130] in which two electron beams accelerated in a gas jet at stage 1 enter another jet at stage 2, and the field of the first beam excites a plasma wave [131] in which the second beam is captured. The net outcome of these processes is an efficient transfer of energy from one beam to the other and doubling the energy in the second beam.

Accelerated electron beams can be generated both at the surface of a solid target and in a supercritical plasma. In a numerical experiment reported in [132], an electron beam outgoing from the target surface was generated by its oblique irradiation with a linearly polarized high-intensity laser pulse. The electron energy at the pulse intensity 4×10^{19} W cm^{-2} amounted to 20 MeV. It was proposed in [133] to generate ultrashort (~ 1 fs) electron beams in the relativistic self-induced transparency regime. Numerical simulation assuming the normal incidence of a circularly polarized 10^{22} W cm^{-2} laser pulse on a plasma layer with the density 10^{21} cm^{-3} demonstrated an electron beam with an energy of the order of 1 GeV that propagated in the direction opposite to the laser radiation.

3.3 A gamma source from laser electron acceleration

The majority of the schemes considered in Section 3.2 do not require high radiation intensities and are operational at a radiation source intensity level of 10^{20} W cm^{-2}. The practical interest in the creation of compact electron-beam laser accelerators is largely attributable to the possibility of using them as the first section of traditional linear accelerators and obtaining short electromagnetic pulses within hard-to-realize ranges. An increase in the intensity to 10^{22} W cm^{-2} would allow generating electromagnetic radiation in the gamma range. An important advantage of laser acceleration is the possibility of using the same laser pulse that accelerated electrons to generate radiation. This advantage is used in a putative scheme for producing gamma radiation, considered in detail below.

This scenario includes three stages. First, a short (about 10 periods) 10^{22} W cm^{-2} laser pulse interacts with a plasma target in which the electron concentration is close to the critical one at a given radiation frequency. Such targets can be made of a thin metal foil preliminarily ionized with a certain delay by another laser, such that the electron concentration decreases to $10^{20}-10^{21}$ cm^{-3} by the time the main pulse arrives. The interaction gives rise to a bubble-like structure in which the electron beam being formed is effectively accelerated to multi-GeV energies. Due to the relatively high concentration of the background plasma, a rather large number of electrons are trapped in the beam ($10^{11}-10^{12}$). Moreover, a wakefield plasma wave is virtually absent in the chosen interaction regime, which ensures a high (20–30%) efficiency of the energy transfer from the laser pulse to electrons. At the second stage, the laser pulse is reverted. For this, at one end of the plasma target, a solid plate is installed that almost instantaneously produces high-density plasma in response to ionization; as a result, the incident laser pulse is totally reflected. The normal incidence prevents the loss of energy to heating the electrons of the solid-state target, while the use of circularly polarized radiation precludes generation of higher-order harmonics upon reflection. Taken together, these make the reversal of the laser pulse maximally efficient. At the third stage, the reversed pulse interacts with the beam of accelerated electrons that remained behind it during acceleration. Due to the high electron energy and pulse intensity, an extremely intense synchrotron emission of electrons in the gamma range takes place, up to the quantum energies $\hbar\omega \sim 1$ GeV. Under these conditions, about 1% of the electron beam energy is converted into gamma radiation. An advantage of this scenario is its self-consistency. It is necessary to ensure the pulse propagation normally to the plane of the reflecting foil. If this condition is satisfied, the reversed laser pulse automatically crosses the electron beam, which obviates the difficult problem of synchronization of laser and electron pulses in time and space. In what follows, each of the three stages is considered separately.

3.3.1 Electron acceleration. A characteristic picture of the interaction between laser radiation and transparent plasma obtained by three-dimensional numerical simulation is illustrated by Fig. 2. The calculated window size is 60 μm in the direction of the x axis and 40 μm in the direction of the y and z axes. The size of the calculated grating is $512 \times 256 \times 256$. The pulse propagates from left to right in the direction of the x axis. The radiation wavelength is 1 μm. Initially, the pulse has a Gaussian profile in both the longitudinal and transverse directions. The pulse half-intensity diameter is 10 μm, and the duration is 10 field periods (about 33 fs). The dimensionless amplitude is $a_0 = 60$ (in agreement with the intensity 9.9×10^{21} W cm^{-2}). The focal plane coincident with the left window edge is 10 μm from the beginning of the plasma layer. The density in the layer is $N_e = 3.3 \times 10^{20}$ cm^{-3} (thrice as low as the critical one). Au_{197}^{10+} ions are mobile. The starting plasma is electrically neutral. The initial particle distribution over velocities is Maxwellian at the temperature 1 keV. Each cell initially contains 10 electrons and one ion. The window begins to move $t = 180$ fs after the onset of calculation.

Evidently, the incoming laser pulse 'sweeps up' part of the plasma electrons and transversely pushes apart the remaining ones. In this process, electrons lock together at the back of the pulse and a small electron-free cavity forms behind it. Such a structure is referred to as a bubble in the literature. Because ions have no time to follow electrons due to the difference in mass, charge-separating fields are formed comparable to the electric fields of laser pulses (of the order of 10^{12} V cm^{-1}). When the bubble closes, part of the electrons are trapped within the newly formed structure and start to move together. Because the plasma is transparent and the pulse strongly relativistic (which additionally reduces the effective plasma frequency), the bubble propagates at a speed comparable to the speed of light. The trapped electrons almost instantaneously gain ultrarelativistic energies and also move with a sublight velocity, thus maintaining synchronism with the accelerating field. As follows from the calculation, the electrons move somewhat ahead of the acceleration phase after they acquire a certain energy until acceleration is arrested. However, other electrons penetrate into the bubble from the plasma to be likewise accelerated to ultrarelativistic energies. In this way, plasma electrons are continuously fed into the beam and its total energy increases continuously. The results of the calculation suggest the complete absence of a trace behind the bubble.

Figure 3 illustrates time dependences of the distribution of the electromagnetic field energy (with the main contribution coming from the laser pulse field), the electron energy spectrum, the total electromagnetic energy, and the electron energy. In addition, Fig. 3c shows the total radiation energy that could be obtained if the pulse were reflected at this moment.

As the pulse propagates in the medium, the number of electrons in the bubble increases and the pulse energy decreases, a characteristic feature being 'erosion' of the pulse leading edge. It follows from Fig. 3a that the instant close to the complete decay of the pulse is optimal for reflection. At this instant, the beam contains 10^{11} electrons, and its total energy is about 10 J.

3.3.2 Pulse reflection. The next stage is pulse reflection at the end of the rarified plasma layer. For this, a sufficiently thick solid target, e.g., metal foil, may be used. The reflection should be as efficient as possible and the loss of energy in the pulse reduced to a minimum. It is well known that the interaction of superstrong radiation with a target is accompanied by matter heating [36, 134–136], resulting in a low energy of the reflected signal. The influence of this factor may be significantly decreased by using a circularly polarized pulse and ensuring strict perpendicularity of its propagation direction to the metal mirror surface.

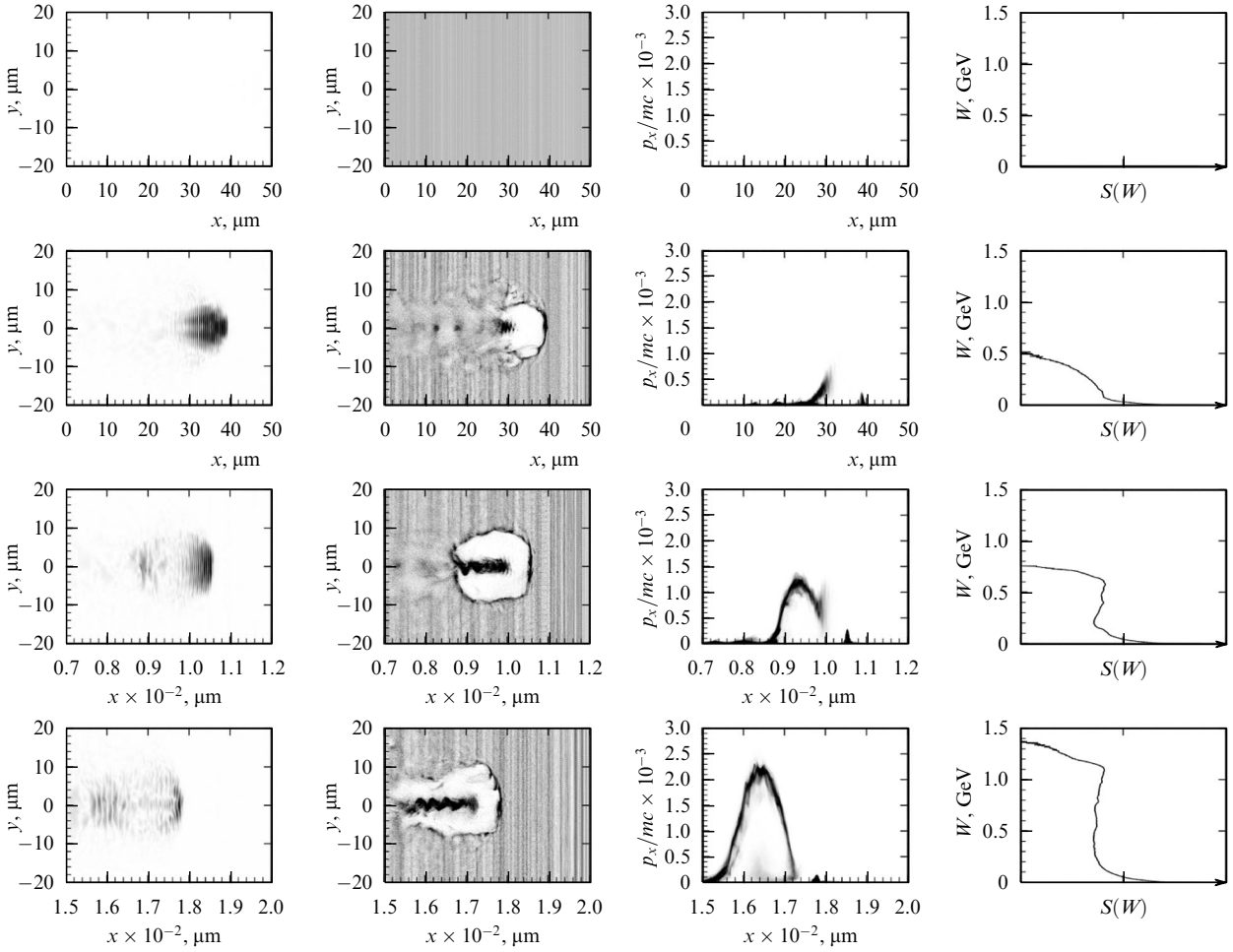

Figure 2. Electron acceleration by a laser pulse in the bubble regime. First column: field distribution E_z in the cross section $z = 0$; second column: electron density distribution; third column: electron phase portrait integrated over transverse momenta and coordinates; fourth column: electron distribution over energies in a logarithmic scale.

Another important issue is the choice of the mirror starting position. If the mirror is too close to the pulse entrance to the rarified plasma, the electrons being accelerated cannot gain sufficient energies; if it is located too far away, the laser pulse energies are insufficient to deliver it to the mirror. In either case, the efficiency of further energy conversion into gamma radiation energy is suboptimal. In other words, the mirror should be properly positioned if the maximally possible radiation energy is to be obtained. The search for such an optimum is a difficult task, being dependent on the plasma concentration, pulse energy, and intensity. In the above example, the optimal mirror position is 200 μm from the entrance of the laser pulse to the plasma.

3.3.3 Pulse-electron collisions. The most important stage is the third one, at which a major fraction of gamma radiation is generated. The possibility of generating gamma quanta in the interaction between superpower laser radiation and high-energy electron beams was considered in several experimental studies. [137–139]. Electrons were accelerated in the traditional SLAC (Stanford Linear Accelerator Center) machine, whose integration with a terawatt laser encountered some difficulty. Such a problem does not arise in the scheme under consideration because it uses a single pulse.

The efficiency of gamma-ray generation in the interaction between superpower laser radiation and an electron beam propagating against the pulse is easy to assess. In the one-dimensional approximation, in accordance with the law of canonical momentum conservation and neglecting the radiation decay force, the transverse electron momentum is determined by the vector potential amplitude at a given point: $\mathbf{p}_\perp = e\mathbf{A}_\perp/c$ ($e > 0$ is the elementary charge). With the above parameters, $p_\perp$ does not exceed 20–30 MeV s^{-1}, while $p_\parallel > 1000$ MeV s^{-1} for the longitudinal pulse. Therefore, the inequality $p_\perp \ll p_\parallel$ is satisfied with a sufficiently good accuracy, which means that the electron interacting with the laser pulse continues to move in the same direction, undergoing only mild transverse 'jerks.' As is known, a relativistic electron undergoing acceleration effectively emits high-frequency quanta, i.e., synchrotron radiation [140]. The spectrum of this radiation is extremely wide, extending up to the cut-off frequency determined by the energy of the electron being accelerated and the magnitude of acceleration:

$$\omega_c = 3\gamma^3\left(\frac{c}{\rho}\right), \qquad (1)$$

where γ is the electron relativistic gamma-factor and ρ is the curvature radius of the electron trajectory. In the case being

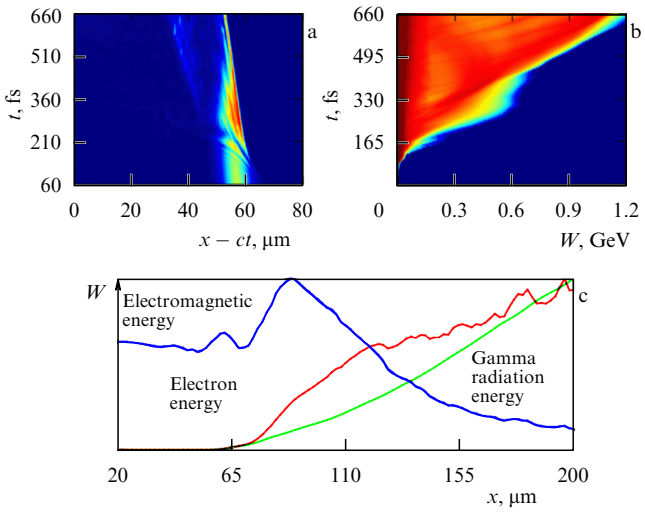

Figure 3. (a) Distribution of the electromagnetic field energy in the calculated window, (b) electron energy spectrum depending on time from the onset of calculation, (c) curves showing time dependences of the total electromagnetic energy, the electron energy, and the total radiation energy that could be obtained if the pulse were reflected at this moment.

discussed,

$$\gamma = \left[1 + \left(\frac{p_\perp}{mc}\right)^2 + \left(\frac{p_\parallel}{mc}\right)^2\right]^{1/2} \approx \frac{p_\parallel}{mc}\,, \tag{2}$$

$$\rho = \frac{\gamma mc^2}{2eE_\perp} \approx \frac{p_\parallel c^2}{2e\omega A_\perp}\,, \tag{3}$$

where ω is the circular frequency of laser radiation. Hence, the cut-off frequency is

$$\omega_c = 6\left(\frac{p_\parallel}{mc}\right)^2 \frac{eA_\perp}{mc^2}\,\omega \sim p_0^2 a_0 \omega\,, \tag{4}$$

where the dimensionless longitudinal momentum $p_0 = p_\parallel/mc$ and laser pulse amplitude $a_0 = eA_\perp/mc^2 = eE_\perp/m\omega c$ are introduced. For the problem in question, $p_0 \approx 2 \times 10^3$, $a_0 \approx 50$, and $\hbar\omega \approx 1$ eV. Therefore, the emission of quanta with energies up to $\hbar\omega_c \approx 2 \times 10^8$ eV $= 0.2$ GeV is possible. The corresponding wavelength is $\lambda \approx 5 \times 10^{-15}$ m. Evidently, the radiation wavelength lies in the gamma range and is significantly smaller than the distance between electrons. Hence, the single-particle approximation implicitly assumed in the derivation is valid. The energy of a single emitted quantum is generally comparable to the electron energy, which suggests the quantum nature of this radiation; for simplicity, however, we restrict ourself to the classical approximation, with the understanding that corrections must be produced by a quantum analysis. Moreover, because the quantum energy is much higher than the electron rest energy, there is a high probability of the generation of electron–positron pairs in the problem under consideration. This effect is also neglected.

We find the energy transmitted into radiation using the known expression for the radiation friction force acting on an ultrarelativistic particle [141]:

$$f_x^{\rm rad} = -\frac{2e^4\gamma^2}{3m^2c^4}\left[(E_y - H_z)^2 + (E_z + H_y)^2\right]. \tag{5}$$

For a circularly polarized pulse propagating oppositely to the x-axis direction,

$$f_x^{\rm rad} = -\frac{8e^4\gamma^2 E_\perp}{3m^2c^4} \sim -kr_e p_0^2 a_0^2 mc\omega\,, \tag{6}$$

where $k = \omega/c$ is the wave number and $r_e = e^2/mc^2$ is the classical electron radius. For the optical range, $kr_e \approx 10^{-10}$. We compute the fraction of the kinetic energy to be lost by an electron via emission in the zeroth approximation (neglecting the effect of the radiation friction force on the electron motion):

$$\eta \equiv \frac{f^{\rm rad} c t_{\rm int}}{(\gamma - 1)\,mc^2} \sim kr_e p_0 a_0^2 \omega t_{\rm int}\,, \tag{7}$$

where $t_{\rm int}$ is the electron–radiation interaction time. Assuming this time to be $\omega t_{\rm int} \sim 10$, we have $\eta \sim 0.01$. It is easy to calculate that about 0.1 J of the energy is converted into gamma radiation in the presence of 10^{11} electrons with the mean energy 1 GeV. The duration of a gamma-ray burst determined by the time of interaction between a laser pulse and a bunch of accelerated electrons is about 10 fs. Clearly, such a source has a record high light intensity: 10^{27} photons every second per 1 mm^2 mrad^2.

4. Ion acceleration: the search for optimal regimes and targets

4.1. Target normal sheath acceleration

Studies on the acceleration of protons and light ions have a shorter history than the electron acceleration research. One of the earliest experiments to observe laser-driven ion acceleration was performed on the petawatt Nova laser at the Lawrence Livermore National Laboratory [142]. In this experiment, a 0.5–5 ps pulse with the intensity 3×10^{20} W cm^{-2} was used to irradiate a solid target. It caused the induced proton beam containing 3×10^{13} particles with energies up to 55 MeV to fly away from the back side of the target; the particles showed a quasi-Maxwellian distribution over velocities with the mean energy of several MeV. This result was interpreted in terms of the so-called target normal sheath acceleration (TNSA) mechanism [143, 144] based on the effective electron heating during laser–target interaction (around 40–50% of the laser energy was absorbed by electrons in the above experiment); the electrons flew apart in all directions, passed through the target, and escaped from its back surface. They formed a negatively charged cloud in the near-surface layer, thus giving rise to a quasistationary electric field. The resulting potential difference was enough to accelerate protons and other light ions from the target. The first experiments thus designed yielded wide quasithermal distributions of accelerated ions over energies, whereas most applications require monoenergetic beams.

The generation of a monoenergetic ion beam was first demonstrated in experiments reported in 2006 [145, 146]. The authors used targets from heavy metal foils (titanium, gold, palladium) with a thin coating on the back side (either a layer of natural organic contaminants or an artificial polymer layer, both containing light ions — protons and carbon). As the acceleration potential was formed, it first accelerated the light ions, whereas the heavy ones contained in the foil remained at rest during the laser pulse action. Because the

ions being accelerated were initially in virtually identical conditions, their dynamics did not differ significantly; this accounted for the monoenergetic spectrum of these ions. A proton beam with energies 1.2 ± 0.3 MeV was obtained in the experiment, i.e., the spread was roughly 25%.

A few methods have been proposed to improve the acceleration efficiency. One was to use microstructured targets to enhance the efficiency of energy transfer from the laser pulse to hot electrons. In Ref. [147], the reflection of a laser pulse was reduced by using a perforated foil with the half-wavelength hole size. It allowed significantly increasing the absorption of the laser pulse energy and, accordingly, increasing the ion acceleration energy. Optimization of the hole size in [148] resulted in the conversion of 16.7% of the laser energy into the energy of accelerated ions. It was proposed in [149] to set an additional foil normally to the front edge of the vertical target. In this case, a laser pulse propagating along the horizontal foil surface effectively accelerated its electrons. Simultaneously, absorption of the laser energy by the plasma increased. A similar design was employed in [150], but thick foil with a narrow channel was attached to the accelerating layer. A laser pulse traveling along the channel accelerated surface electrons in the direction of its propagation.

4.2 Acceleration by light pressure

Despite the relative success of the TNSA design, other scenarios are preferable at high intensities that cannot be realized at low ones. Worthy of mention is the so-called laser-piston regime proposed in 2004 (also known as the light sail regime). It is based on the idea of body acceleration by light pressure, suggested in the early 20th century [152]. In the original design, a thin hydrogen foil was irradiated by a laser pulse with the intensity 10^{23} W cm^{-2} that torn out a bunch of plasma composed of electrons and ions to accelerate it as a whole. A numerical simulation showed the possibility of obtaining protons with energies of several GeV in this regime. The same authors proposed a simple model of the ion layer acceleration based on the assumption that the layer was accelerated as a whole by laser pulse pressure. We note that due to the Doppler effect, a reflected pulse has a much lower frequency than the incident one; this allows transmitting practically 100% of the incident radiation energy to the layer. This model was used to evaluate the final ion energy in the layer depending on the acceleration time. In the ultrarelativistic case, it has the form

$$E_{\mathrm{i\,kin}}(t) \approx m_{\mathrm{i}}c^2\left(\frac{3E_{\mathrm{L}}^2 t}{8\pi n_{\mathrm{e}} l m_{\mathrm{i}} c}\right)^{1/3}, \qquad (8)$$

where m_{i} is the ion mass, E_{L} is the electric field amplitude in the laser pulse, n_{e} is the initial electron concentration in the layer, and l is the initial layer thickness. For a 25 fs Gaussian pulse with the maximum intensity 1.37×10^{23} W cm^{-2} used in the calculation, the estimate is $E_{\mathrm{i\,kin}} \approx 30$ GeV for a 1 μm thick foil with the electron density 10^{22} cm^{-3}.

A similar idea may be used to accelerate ions at the leading edge [153–166]. This scenario is based on the normal incidence of a circularly polarized pulse onto a solid-state target. Circular polarization ensures the absence of noncollisional heating, while normal incidence is responsible for quasistationary acceleration in which electrons are pushed by the ponderomotive force and give rise to an acceleration potential, under the effect of which ions at the leading edge acquire an energy proportional to the laser pulse amplitude [157]. A study of the dependence of the acceleration efficiency on the plasma density revealed an optimal electron concentration at which the energy of the ions being generated reached its maximum [158]. Later [159], this regime was modified by making it possible to reuse the layer. At the first stage, the pulse accelerated the stationary layer; when it came up to the end of the layer, it began to accelerate the previously accelerated ions, thus further increasing their energy. Bearing in mind the small thickness of the layer, this regime can be reduced to the above idea of thin film acceleration by light pressure. It is essential that the use of a circularly polarized pulse permits reducing the radiation intensity, as is necessary to realize this scenario [160]. Its other peculiar feature is that all the ions receive equal energy. The scenario has the advantages such as high efficiency, a high density of ion bunches, low divergence, and a short (fs) duration of the beam [161]. The scheme was optimized in [162, 163]; an optimal thickness was found at which only a thin ion layer at the rear edge of the target undergoes acceleration.

A drawback of this scenario is that it is vulnerable to transverse Rayleigh–Taylor [164] or smaller-scale [165, 166] instabilities, which may enhance translucence of the layer and arrest acceleration. However, it was shown that these instabilities may be suppressed by making the motion of the accelerated layer ultrarelativistic [167]. Moreover, a specially profiled laser pulse [168] or a target [169] can be used. Also, stabilization of the layer may be achieved by virtue of edge effects [170] or by the addition of the initial stage of pulse self-channeling [171]. It was proposed to use a two-component target [172] composed of carbon and hydrogen ions. In this case, the lighter hydrogen ions form a thin layer accelerated mainly by Coulomb forces originating from the carbon ions that form a dense plasma cloud due to the Rayleigh–Taylor instability. The hydrogen ion layer proves to be stable because it overlies a 'heavier' liquid of carbon ions; by contrast, in a monocomponent target, protons occupy the 'surface' of a 'lighter' photon liquid.

Acceleration by light pressure remains poorly studied in experiment because it requires high radiation intensities to be realized. Two series of experiments were conducted in 2008 at the sub-petawatt Vulcan RAL facility [173]. Laser pulses with the energies 60 and 250 J and respective durations 1 and 0.7 ps were used. The focused intensity varied from 3×10^{19} W cm^{-2} to 2×10^{20} W cm^{-2}. Irradiation of 2 μm and 5 μm thick aluminum and copper foils with such pulses induced proton beams to fly out from the back side of the targets. They were peculiar in that their low-energy portions showed relatively low divergence and were emitted from a small spot, in sharp contrast to what occurred in the TNSA regime. These observations suggested that ion acceleration was due to light pressure; this conclusion was confirmed by numerical simulation. Experiments at the 20 TW facility at the Max Born Institute, for the first time using a circularly polarized 45 fs laser pulse with the wavelength 810 nm and energy 1.2 J were reported in 2009 [174]. The double plasma mirror technique [175] enabled the experimenters to reach a pulse contrast of the order of 10^{11} at times less than 10 ps. This allowed interaction between a laser pulse and the intact ultrathin targets (2.9 to 40 nm carbon films). The authors observed formation of a monoenergetic beam of carbon ions C^{6+} with the energy 30 MeV. Interaction with the 5.3 nm foil proved optimal. The two results are consistent with both an early theoretical prediction and the numerical simulation in [175].

4.3 Acceleration by ponderomotively pushed electrons

Acceleration by ponderomotively pushed electrons is based on a similar principle [176]. The idea is to create a charge-separating field in a thin layer of a heavy metal by pushing electrons toward the back edge of the target by ponderomotive forces. The main problem is to produce as large a potential difference as possible in order to accelerate light probe ions crossing the entire layer. In other words, the present design, unlike traditional ones, implies that the ions to be accelerated should initially be located at the start of the layer.

The optimal interaction regime was found based on the approach developed in [177]. It turned out that the energy of accelerated ions at a given intensity reaches a maximum in targets of minimal density. However, the admissible plasma concentration has a lower bound determined by the relativistic self-induced transparency. Given the optimal target parameters, the maximum energy of ions accelerated in such a target is related to the radiation intensity as

$$\varepsilon_{\mathrm{i}}[\mathrm{MeV}] = 0.71 Z_{\mathrm{i}} \times \left(\frac{I\,[\mathrm{W\ cm^{-2}}]}{10^{18}} \left(\lambda\,[\mu\mathrm{m}]\right)^2 \right)^{3/4}, \qquad (9)$$

where Z_{i} is the charge of the ions.

The results of analytic calculations were confirmed by numerical simulation. One-dimensional computation was done based on numerical simulation of the Vlasov–Maxwell set of equations for the three-component plasma composed of electrons and carbon C_{12}^{6+} and gold Au_{197}^{6+} ions, in which different components interacted only via the mean electrostatic field. Irradiation of a composite target was considered. The target consisted of a thin carbon layer ($L_{\mathrm{C}} \approx 0.1\lambda$) and a thick gold layer ($L_{\mathrm{Au}} \approx 1.9\lambda$), with their total electron concentration being constant (equivalent to $n_0 = 10$, where n_0 is the unperturbed concentration related to its critical value at a given radiation frequency, i.e., the so-called overdense parameter). The carbon layer at the plasma surface subject to irradiation was immediately adjacent to the gold layer. The pulse incident on it had a Gaussian envelope with the length equal to six field periods and the maximum intensity $I_{\max} = 2500 I_{\mathrm{rel}}$ (where I_{rel} is the the so-called relativistic intensity, equal to the radiation intensity at which the electron quiver energy in the wave coincides with the rest energy; for circular polarization, $I_{\mathrm{rel}}[\mathrm{W\,cm^{-2}}] = m^2\omega^2 c^3/4\pi e^2 \approx 2.75 \times 10^{18}\lambda^{-2}\,[\mu\mathrm{m}]$), in agreement with the optimal problem parameters at which ions with the energies $\varepsilon_{\mathrm{C}} = Z_{\mathrm{C}} n_0 L^2/2 \approx 4000\, mc^2 \approx 2$ GeV were expected to be produced. The results of the calculation are presented in Fig. 4. The space–time distribution of the ion and electron densities in the layer is shown in Fig. 4a. With these radiation parameters, almost all electrons are pushed toward the rear edge, whereas gold ions remain practically at rest. The resulting potential difference in the layer is close to a maximum. The chosen pulse length enables the ions being accelerated to take an optimal path because they leave the layer at about the instant when the maximum potential difference is achieved. Figure 4b demonstrates the distribution of accelerated carbon ions at the instant $t = 23T$ (the phase plane of the ions and their distribution by pulses integrated over all coordinates). It turned out that a monoenergetic ion beam was generated in the course of the interaction with the pulse $p = 0.5 M_{\mathrm{C}} c$ corresponding to the energy $\varepsilon = 0.12 M_{\mathrm{C}} c^2 \approx 1.4$ GeV. The discrepancy between this and the predicted results is attributable to dynamic interaction effects, e.g., partial translucence of the layer related to finite electron temperature and suboptimal choice of the pulse length.

In a real situation, this acceleration regime may be affected by such factors as the electron heating and extraction by the laser pulse as a result of target destruction or the development of transverse instabilities. The significance of each of these factors was assessed by a comprehensive three-dimensional simulation of the ion acceleration problem using the particle-in-cell (PIC) method realized in the parallel three-dimensional code of the extreme laser matter interaction simulator (ELMIS) developed by the SimLight Group in the Sector of Simulation of Ultrafast Optical Processes, IAP RAS. For the purpose of calculation, the layer was assumed to be 1 μm thick, and its overdense parameter was chosen as $n_0 = 15$. The ions to be accelerated were protons in a 100 nm layer. Gold ions Au_{197}^{10+} formed the background plasma. A Gaussian pulse of the length equal to three field periods and width 8 μm with a carrying wavelength of 1 μm was used. The pulse amplitude at the maximum was $a_0 = 50$. The results are presented in Figs 5 and 6. Similarly to the one-dimensional

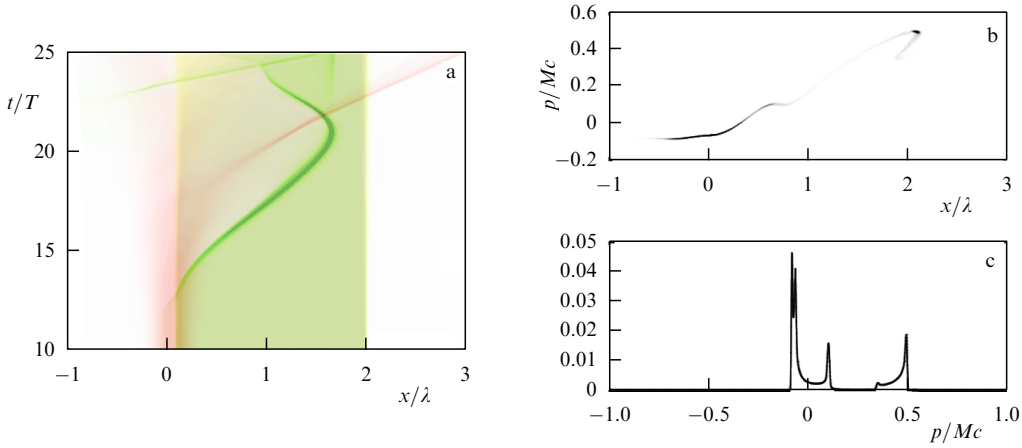

Figure 4. Calculation of the dynamic problem of interaction between relativistically intense laser radiation and a structured plasma layer (in color online). (a) Space–time interaction diagram. Colors indicate the density of plasma components (green — electrons, yellow — gold ions, red — carbon ions). (b) Phase plane of carbon ions at the instant of escape from the layer ($t = 23\,T$). (c) Carbon ion distribution by pulses integrated over coordinates at the same time instant.

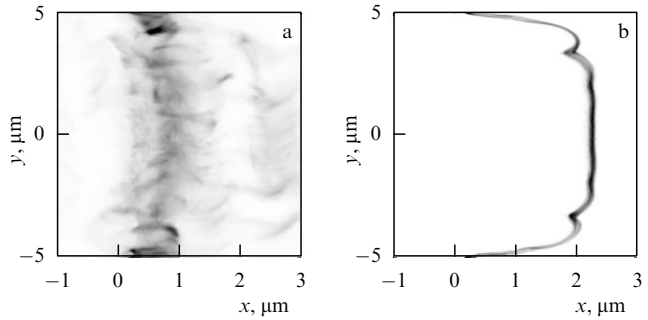

Figure 5. Computations in the three-dimensional problem of the interaction between relativistically intense laser radiation and a structured plasma layer: distribution of electron (a) and proton (b) concentrations.

case, a beam of accelerated protons was formed showing the monoenergetic distribution near the 150 MeV peak. The enlarged peak width is attributable to non-one-dimensional effects and transverse instabilities developing in the plasma layer and deteriorating the structure of the accelerating field. Also noteworthy is a high degree of collimation of the accelerated beam. The angular spread does not exceed a few tens of milliradians.

4.4 Cascade ion acceleration

The above scenario is actually an extension of the acceleration by ponderomotively pushed electrons based on the effect of the relativistically induced slab transparency [178]. This effect occurs in sufficiently thin plasma layers under the action of superstrong circularly polarized radiation. Given the rather high radiation intensity, all electrons may be pushed into a thin electron layer at the end of the plasma layer. The resulting electron layer is thinner than the skin layer. The electron rotation rate within the layer is limited by the speed of light; hence, there is a limitation on its reflectivity accounting for the almost unobstructed passage of laser radiation. The transmitted pulse may be used to create the potential difference in the next layer.

As shown in [178], the degree of electron pushing in a plasma layer subjected to circularly polarized radiation depends mainly on the radiation intensity and increases with it as

$$kz_{\mathrm{b}} \approx \frac{2\sqrt{I}}{n_0}\,, \tag{10}$$

where z_{b} is the coordinate of the pushed electron boundary, k is the wave number in the incident pulse, and I is the radiation intensity normalized to the so-called relativistic intensity. Because z_{b} cannot be greater than the layer thickness, formula (10) gives the threshold intensity value

$$I_{\mathrm{th}} \approx \left(\frac{n_0 kL}{2}\right)^2, \tag{11}$$

where L is the layer thickness. At the above-threshold intensities, all electrons are pushed into a layer thinner than the skin layer. As a result, all plasma electrons start rotating with a sublight velocity. The emissive power of such a layer is limited by the value

$$I_{\mathrm{sat}} = \pi c\sigma^2 = \left(\frac{n_0 kL}{2}\right)^2, \tag{12}$$

where $\sigma = eN_{\mathrm{e}0}L$ is the charge surface density in the layer. Hence, its emissive power is exactly equal to the threshold radiation intensity in (11). When the intensity surpasses the threshold, the transmittance factor can be found from the formula

$$T \equiv \frac{I_{\mathrm{tr}}}{I_{\mathrm{inc}}} = 1 - \frac{(n_0 kL)^2}{4I}\,, \tag{13}$$

where I_{tr} is the intensity of the transmitted wave and I_{inc} is the incident wave intensity.

If a pulse with an above-threshold intensity and a Gaussian profile in the longitudinal direction is incident on the plasma layer, the above argument leads to the following interaction scenario. At the time of arrival of the pulse leading edge and until the incident intensity surpasses the threshold, the energy flux is almost completely reflected from the layer, whose electrons are gradually pushed by the ponderomotive force, giving rise to a longitudinal electric field. As the intensity reaches the threshold level, the transparency regime sets in where electrons cease to be pushed further and the pulsed electromagnetic wave is only partly reflected. Simulation of this process by the PIC method demonstrated the possibility of forming a much higher acceleration potential than that created by pushed electrons. This effect can be observed using very short ($\approx$ 30 fs) laser pulses that quickly pass from the reflection to the transparency regime. In this case, the rapid increase in the outgoing wave intensity leads to the formation of a very sharp leading front of the transmitted

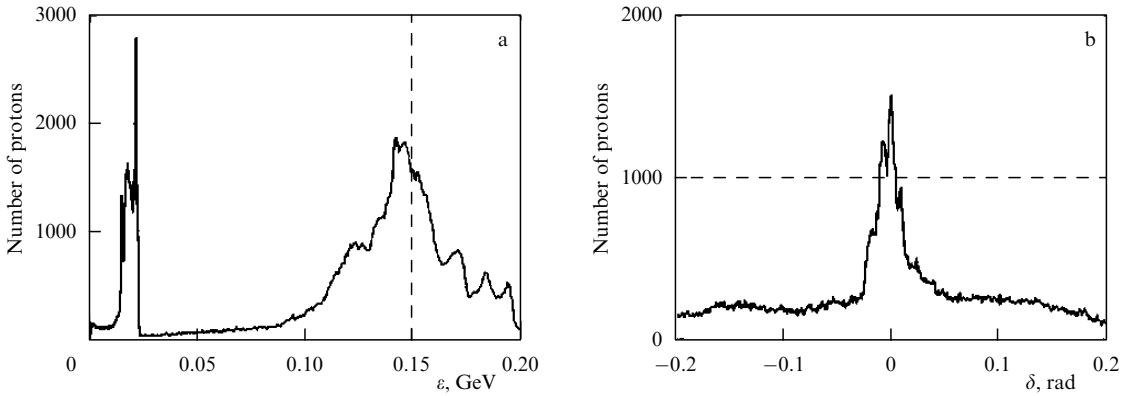

Figure 6. Proton distribution by energies (a) and angles (b) after acceleration in a plasma layer.

pulse, capable, by means of the ponderomotive force, of extracting part of the electrons from the plasma layer and transporting them far away from it. This results in the formation of a charge-separating field outside the layer, which can accelerate ions.

An additional benefit is that the strong heating of electrons at the instant when the layer becomes transparent decreases their reflecting capacity almost to zero, making it possible to reuse the transmitted pulse in the next plasma layer. This mechanism underlies the multi-cascade ion acceleration.

The formation and acceleration of a proton beam on the first plasma layer encountered by a pulse require special consideration. If a highly monoenergetic beam characterized by a small spread over the longitudinal coordinate forms in the first layer, it may further propagate in space, retaining its properties and successively gaining energy at each of the remaining layers. It is equally important that such a proton beam be maximally accelerated starting from the very first layer. This goal can be achieved by the choice of an optimal position of the proton-containing layer in which a laser pulse forms the beam to be accelerated. Also, the problem can be solved by numerical simulation of the interaction between laser radiation and a thin plasma layer, introducing differently positioned probe protons into the calculation. The optimal position of the probes is deduced from the maximum energy of the accelerated particles.

Such a calculation is exemplified by the results presented in Fig. 7. It shows, first, that the optimal position of the layer with the protons being accelerated is at the front rather than the rear wall of the thin foil. Second, the full acceleration potential gradually increases to a maximum during the action of the laser pulse; therefore, for the optimal acceleration to be achieved, protons must be introduced into the accelerating layer some time after the onset of the pulse action to allow the highest acceleration potential to form. The proton beam introduction time can be controlled by varying the size of the gap between the proton-containing and accelerating layers.

Optimization of multi-cascade acceleration implies optimization of the interlayer distance to ensure the passage of the proton beam through the region in which it is accelerated (the accelerating potential difference region) at those time intervals in which the laser pulse causes a maximum decrease in the potential.

Figure 8 presents the results of numerical simulation of the interaction between a circularly polarized relativistically intense laser pulse and a target having five optimally spaced layers. The first layer contained only protons, and the remaining four layers were composed of gold ions Au_{197}^{6+} and electrons. The electron concentration in the first layer corresponded to $n_0 = 10$, and in the remaining ones, to $n_0 = 100$. All the layers were 100 nm thick. The incident pulse had a Gaussian envelope with the peak intensity 10^{22} W cm^{-2} and duration 30 fs. The ion beam that formed on the first accelerating layer passed through all four cascades and was sequentially accelerated in each of them. As a result, the ion distribution by energies at the output had a relatively narrow peak in the vicinity of 200 MeV.

4.5 Alternative scenarios

The following alternative ion acceleration modes are worthy of mention. The acceleration of protons in the cavitation regime of laser pulse propagation in a transparent plasma considered in [179] requires relativistic energies of ions. Therefore, it was proposed to combine this method with pre-acceleration by light pressure [180]. Another option is the so-called breakout afterburner (BOA) regime [181], in which linearly polarized laser radiation interacts with a thin foil heated throughout its volume and destroyed to ensure pulse

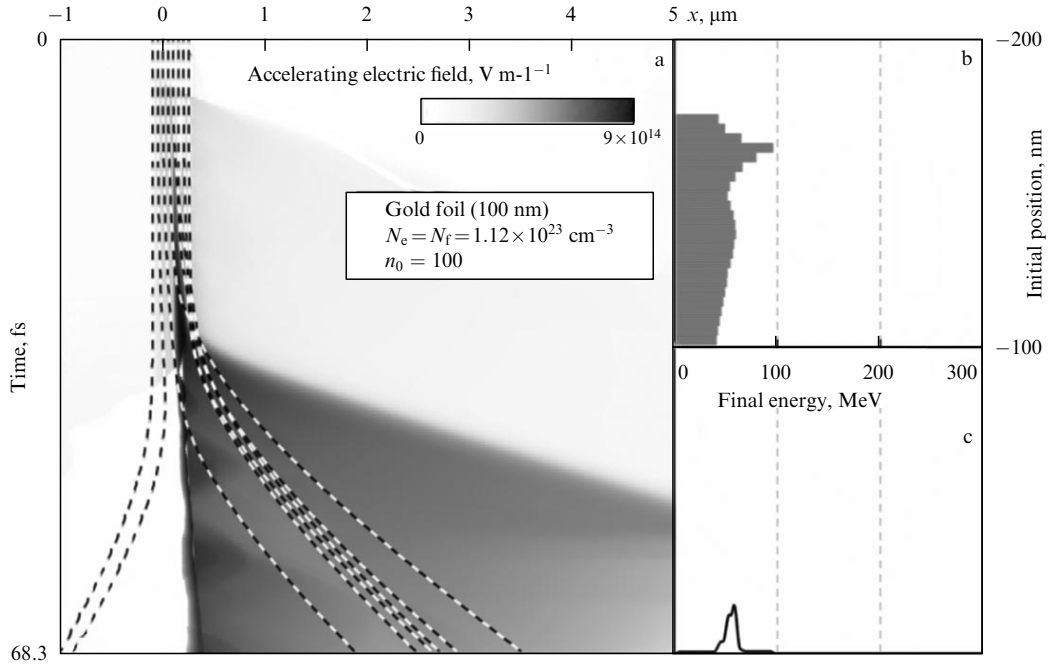

Figure 7. (a) Trajectories of probe particles (protons) initially positioned differently, accelerated by a laser pulse with a Gaussian profile acting on a thin accelerating plasma layer. The longitudinal accelerating field is shown by a color density plot. (b) Diagram showing the dependence of the final proton energy on the initial particle position. (c) The final proton distribution over energies.

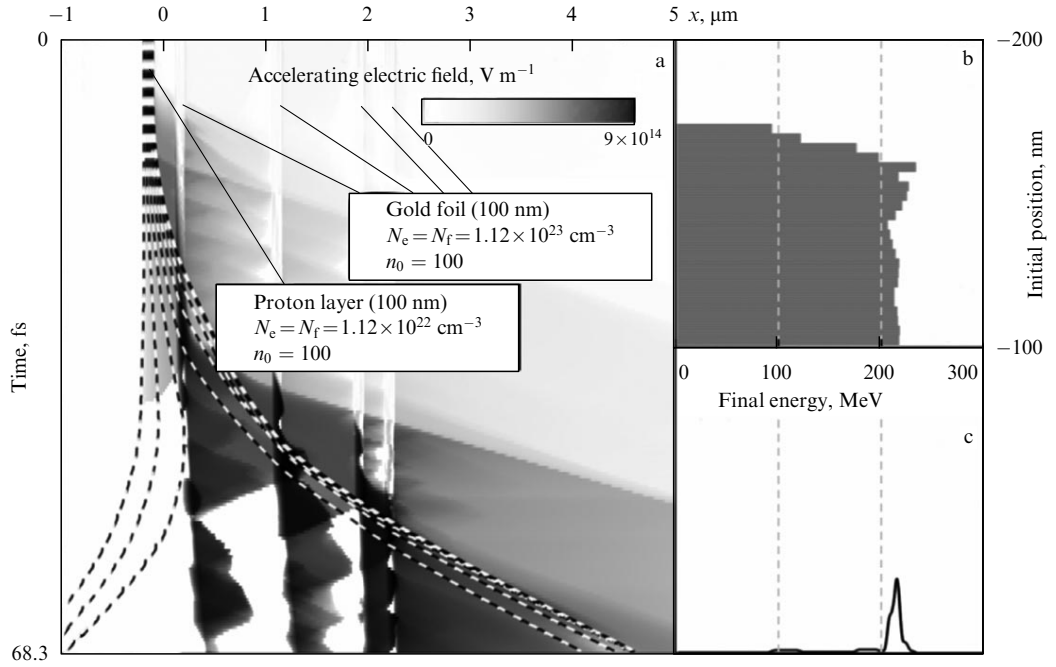

Figure 8. The same as in Fig. 7 for a target made of four accelerating foils. See the text for the calculation parameters.

propagation in the hot plasma. In this case, a relativistic Buneman instability develops [182, 183], leading to efficient energy transfer from electrons to ions.

5. New sources of attosecond radiation

5.1. Generation of higher-order harmonics in a gas

The first generation of sources of attosecond pulses emitted higher harmonics as a result of interactions between laser pulses and gas jets. The production of higher-order harmonics in this process is due to the nonlinear response of atoms to ionization; therefore, the harmonics can be generated despite the relatively low intensities of the order of 10^{13} W cm^{-2} available today [184, 185]. The advent of the CPA technique in the 1990s enabled experimenters not only to observe the generation of tens of harmonics but also to show that their spectrum has a plateau-like structure (see, e.g., [186]). In a few years, the plateau-like structure was explained in terms of a semiclassical model that considered the generation of higher harmonics at each optical period as a three-step process [187]. First, an electron escapes from the atom by tunneling ionization, then it travels far from the ion under the effect of the pulse electric field, and finally it collides with the parent ion to emit a photon. The maximum photon energy is determined by the sum of the ionization potential and the maximum kinetic energy gained by the electron by the time of collision, in accordance with the semiclassical description. This allows finding the boundary of the plateau in the spectrum of higher harmonics.

Another important achievement was the generation of coherent radiation in the 'water window' (the wavelength range between 2.3 and 4.4 nm) finding wide application in biochemistry [188, 189]. In 2008, ultrashort laser pulses only 1–2 optical periods in duration were used to experimentally demonstrate the possibility of generating pulses shorter than 100 attoseconds in gas jets. This result is interesting for the investigation of ultrashort processes in atoms and molecules [190].

Because the most efficient mechanisms of harmonic generation in gases are underlain by transitions between free and bound states, production of higher-order harmonics in gas jets does not require superpower (petawatt) lasers. But it is in this range that the most important practical results concerning the generation of radiation in hard-to-realize ranges with the wavelength up to 1 nm have been obtained in the past 20 years. Nevertheless, the efficiency of generating higher harmonics in gas jets remains rather low, about 10^{-3}%.

The availability of high-intensity laser systems in recent years accounts for increasingly extensive research on harmonic generation in the interaction between laser pulses and solid-state targets aimed at attaining higher efficiency. Such devices constitute the second generation of sources of attosecond radiation.

5.2 The first work with solid-state targets

The generation of higher harmonics on the surface of a solid target in the field of a superstrong laser pulse was first observed at LANL in 1981 [191]. Those experiments were designed to examine the interaction between radiation from a CO_2 laser with the intensity $10^{14}-10^{16}$ W cm^{-2} and solid targets of aluminum, titanium, iron, gold, copper, polyethylene, and Teflon. The reflected signals contained laser frequency harmonics up to the 29th order, their number being dependent on the target material. The first attempt to explain this phenomenon was undertaken in less than a year [192]. The generation of harmonics was accounted for by resonant absorption of the laser pulse energy and excitation of plasma oscillations at multiple frequencies. The natural limit on the number of harmonics was the plasma frequency, lying for most solid-state materials in the range from the 20th through the 30th orders. This was regarded as a serious limitation and has long hampered the development of research in this field.

5.3 Relativistic oscillating mirror model

The situation changed in the mid-1990s, when it was noticed that harmonics can be generated based on the Doppler effect [193]. In this case, the maximum harmonic order determined by the squared electron relativistic factor is not restricted by the plasma density. This prediction was confirmed numerically [194, 195] and experimentally [196, 197]. Somewhat later, a theoretical explanation for the slow roll-off of the harmonic spectrum proposed in [198] provided a basis for the generation of ultrahigh radiation intensities by focusing laser-induced coherent harmonics [199].

The next important step in the study of the mechanisms of the generation of higher-order harmonics was made in [200], where electron emission in the ultrarelativistic limit was shown to have a synchrotronic nature and to occur within a short time interval; as a result, the cut-off frequency of the spectrum being generated is given by the cubed rather than squared relativistic electron factor. This theoretical finding was confirmed in an experiment at the Vulcan facility at RAL [201–203]. This experimental series demonstrated the generation of X-rays with the quantum energy up to 3.5 keV in a solid target irradiated by a laser pulse with the intensity 2.5×10^{20} W cm^{-2}, duration 500 fs, and contrast $10^{10} : 1$ at times ≈ 10 ps. It turned out that such a system makes up an ultrahigh-brightness source producing $> 10^{22}$ photons in 1 s per mm^2 mrad^2 over 0.1% of the spectrum width for wavelengths shorter than 4 nm. Moreover, a relatively high efficiency of energy conversion into harmonics was documented.

In was shown in 2008 by numerical simulation [204] that at certain parameters, the radiation spectrum may be flatter than predicted by the theory proposed in [200]. An attempt to explain this effect was undertaken in [205]. Numerical calculations performed there suggest that the main cause of such spectrum behavior is the formation of a nanosize electron beam flying out in the direction opposite to the laser radiation. Its thickness is so small that individual electrons coherently generate synchrotron radiation and thereby markedly enhance the intensity of higher-order harmonics.

Of special interest as regards harmonic generation is the possibility of obtaining attosecond pulses [206]. It was first noticed in 1998 in the interaction of strong laser radiation with solid-state plasma [207]. Since then, several scenarios for generating attosecond pulses have been proposed, such as selective filtration of radiation [198, 208–210] and the use of ultrahigh strongly focused pulses [211] and laser pulses with variable polarization [200, 212]. As shown in experiments reported in 2009 [213], harmonics are generated synchronously, which implies the possibility of generating a sequence of attosecond pulses. However, such filtration has not yet been accomplished in experiment.

5.4 Relativistic electron spring model

A most intriguing objective of the conversion of light emission into attosecond pulses is to generate ultrahigh intensities in order to observe the effects of vacuum nonlinearity. According to recent assessments and calculations [214], intensities of the order of 10^{26} W cm^{-2}, i.e., three orders of magnitude higher than those expected to be achieved in the near future in the framework of some international projects [215], are needed to observe the avalanche-like production of electron–positron pairs. One obvious way to enhance the intensity is to use a shorter wavelength in order to reduce the volume in which the energy is concentrated at the limiting focusing bound by the diffraction limit. Apart from the regime with focusing attosecond pulses generated at a spherical plasma surface [199], it was proposed to focus the oncoming laser pulse reflected from an electron mirror moving with a relativistic speed and resulting from the break of a wakefield wave [216] or from the ponderomotive expulsion of electrons from thin films [217]. Practical realization of all these ideas is strongly hindered by the relatively low efficiency and poor spatial coherence of the generated radiation.

The idea to generate high-power attosecond pulses by oblique irradiation of the overdense plasma surface looks very attractive as a means of enhancing the energy transformation efficiency [204, 205]. This regime is characterized not only by a flatter harmonic spectrum but also by the fact that an attosecond pulse generated at each period has a larger amplitude than the amplitude of radiation incident on the plasma. This implies not only conversion of the laser pulse energy into the energy of higher-order harmonics but also concentration of the energy of a single optical pulse period in an attosecond burst.

Redistribution of the energy in nonlinear laser–plasma interactions is not taken into account in the relativistic oscillating mirror model [193] that postulates the equality of the amplitudes of incident and reflected radiation at a certain effective point at each instant of time.

It is convenient to analyze energy conversion during oblique irradiation of a plasma surface by reducing the problem to one dimension and passing to the reference frame moving along the surface (Fig. 9) with the speed $c \sin\theta$, where θ is the incidence angle. The ponderomotive force exerted by an electromagnetic wave incident on the layer causes electrons to penetrate deep into the plasma. In the case of oblique incidence, contrary to that of normal incidence, the presence of a plasma flow in a moving reference frame results in a magnetic field created by stripped ions when electrons go deep into the plasma. This in turn accounts for the difference in the ponderomotive action of the wave on electrons at two field half-periods. During the half-period when the electric field is parallel to the y axis, the electron pulse increases in the direction opposite to the axis orientation, and the Lorentz force from the magnetic field created by stripped ions displaces them farther from the boundary. In this way, a thin current-carrying electron layer (nanosize beam) is formed whose charge and current densities are much higher than their initial values in the plasma. The appearance of internal fields in the plasma and acceleration of a part of the plasma electrons lead at this stage to accumulation of the incident wave energy by the plasma. In the case of linear polarization, the force of light pressure oscillates during the

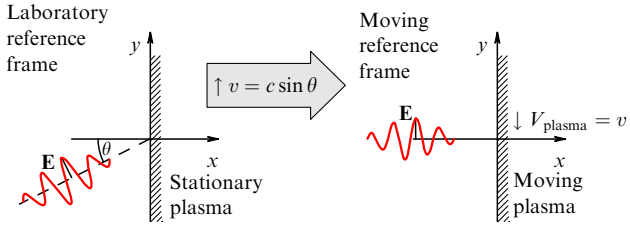

Figure 9. Reduction of the problem of oblique irradiation of the plasma surface to one-dimensional geometry when passing to a moving reference frame.

field period. As a result, the charge-separating force at a certain instant causes the nanosize beam formed of displaced electrons to 'break loose' and fly against the incident wave; it thus becomes a source of an attosecond burst. The energy accumulated at the first stage is flashed out for a time of the order of a few tens of attoseconds. Such a three-stage description of the process is called the relativistic electron spring model [218] because it resembles the scenario of energy accumulation in a mechanical spring.

The analytic model developed in [218] for the description of the above process is based on three postulates. First, it assumes that plasma electrons can be at each instant represented in the form of two components. One is an infinitely thin layer of pushed electrons at a certain moving point x_s, containing all particles from the region $0 < x < x_s$; the other includes electrons with the unperturbed concentration at $x > x_s$. Second, it is assumed that electrons in the layer move at speeds close to the speed of light, which means that their motion is characterized only by the direction. Together with the first assumption, this implies that the electrons have equal speed components not only along the x axis but also along the y axis, and the z-component are zero due to the absence of forces along the z axis. Finally, it is assumed that the electron layer together with the flux of uncompensated ions in the region $0 < x < x_s$ totally compensates the incident electromagnetic radiation in the unperturbed region $x > x_s$.

Based on these assumptions, it is possible to derive a first-order ordinary differential equation for the time evolution of the layer $x_s(t)$ and to express the direct profile of a signal emitted in the direction opposite to the x-axis direction in terms of $x_s(t)$. Comparison of the results of numerical simulation by the PIC method and by numerical integration of the differential equation derived in the framework of the theory in question indicates that the model describes the profile of the reflected signal at ultrarelativistic intensities of the order of 10^{23} W cm^{-2} with good accuracy. As follows from the model, this profile is determined only by two dimensionless parameters, the angle θ of wave incidence onto the plasma surface and the so-called relativistic similarity parameter S (given by the ratio of the plasma density normalized to the critical density to the incident wave amplitude normalized to the relativistic amplitude). Further development of the analytic theory may help determine both the duration and the amplitude of attosecond pulses being generated by taking the degree of the coherence of the electron layer emission into account.

Characteristics of attosecond pulses obtained by numerical simulation using the PIC method and in the relativistic electron spring model are compared in Fig. 10. It shows that the most intense attosecond pulses are generated in a region of optimal parameters with the center at the point

$$\theta_g \approx 62^\circ, \quad S_g \approx \frac{1}{2}. \tag{14}$$

The existence and the particular form of optimal conditions (14) are predicted by a theoretical model from the detailed analysis of the differential equation for $x_s(t)$ by methods of the qualitative theory of nonlinear differential equations; the point defined by (14) on the plane of parameters S and θ corresponds to a triple bifurcation point for three possible regimes (Fig. 11a).

The difference between the regimes can be illustrated by qualitatively depicting the trajectories of electron motion in the layer in response to the emission of an attosecond pulse in the moving reference frame (Figs 11b–e). The direction to the observer shown in the figure is understood as the direction normal to the plasma surface in the moving reference frame. In the case of relativistic motion, the charged particle emission pattern shows two narrow lobes 'pressed' in the direction of motion. Therefore, given the trajectory in Fig. 11b, the reflected signal is shaped as two bipolar bursts, each corresponding to the instant at which the electron moves exactly in the direction of the observer. If the second instant of radiation falls within the region with $x < 0$ (Fig. 11c), which does not satisfy the model assumptions, the second bipolar burst is absent. Finally, if the trajectory is as shown in Fig. 11d, then one of the lobes corresponds to emission and the profile has the form of a unipolar pulse. At the triple bifurcation point, the trajectory is shaped as in Fig. 11e. In this case, the electron emits for an especially long time with a maximum amplitude, thus creating optimal conditions for coherent radiation by all electrons present in a layer of a small but finite size. Because the coherence plays a key role, it is this case that corresponds to the maximum amplitude of the attosecond pulse being generated.

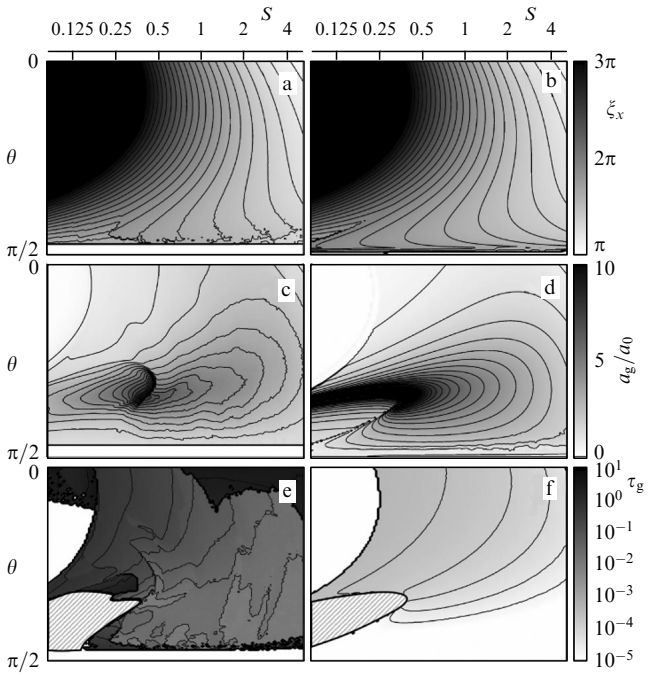

Figure 10. Generation phase ξ_g, the amplitude a_g/a_0, and the duration τ_g of the attosecond pulse obtained in the framework of the relativistic electron spring model (b, d, f) and by numerical simulation of semibound plasma irradiation by a single period of a 1 μm wave with the intensity 10^{23} W cm^{-2} (a, c, e). Hatched areas in diagrams (e, f) are unipolar pulse generation regions.

Theoretical analysis of the shape of attosecond pulses shows that the harmonic spectrum decreases exponentially with a characteristic scale $\sim \gamma^3$ (γ is the electron layer gamma-factor) to the harmonics corresponding to the radiation coherence limit. Because $\gamma \gg 1$, the harmonic spectrum in the case of coherent radiation is much wider than the spectrum with the power-law fall-off factor $-8/3$ predicted by the relativistic oscillating mirror model [200].

Under optimal radiation conditions (14), electrons from the plasma surface emit attosecond pulses with an amplitude one order of magnitude higher than the amplitude of incident radiation. Such an efficient method for the transformation of

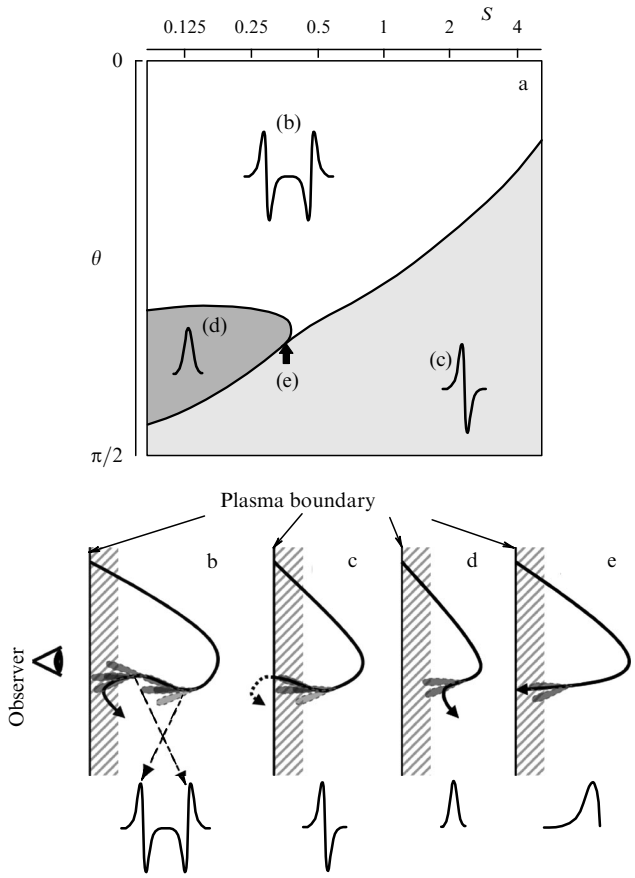

Figure 11. (a) Regions on the plane of parameters S and θ corresponding to qualitatively different regimes of pulse generation. (b–e) Schematic representation of the trajectories of electrons in a nanosize layer, their emission pattern at the moments of maxima generation, and the corresponding pulse being generated.

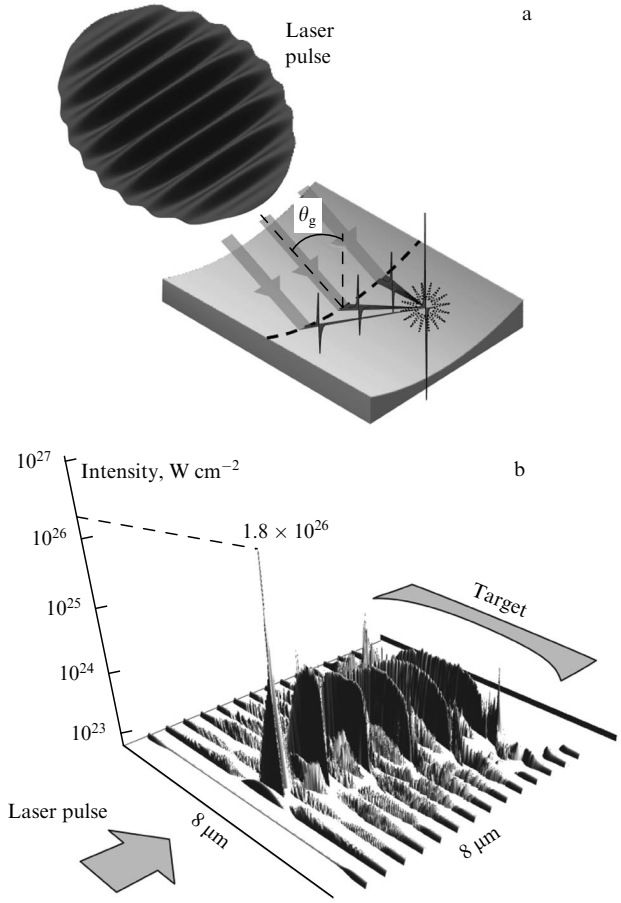

Figure 12. (a) Schematic illustration of the concept of using a target in the form of a trough to generate intensities needed to observe effects of vacuum nonlinearity. (b) Intensity distribution at the instant of focusing giant attosecond pulses generated on the target surface obtained by numerical simulation in the reference frame moving along the trough guide. Simulated oblique irradiation of the target with the electron concentration 10^{23} W cm^{-2} by a polarized laser pulse with the intensity 10^{23} cm^{-3} at the optimal angle $\theta_g = 62°$. The ELMIS parallel code [219] was used.

optical radiation to the attosecond one can be used to create fields required for observing vacuum nonlinearity effects. The concept expounded in [218] is based on the use of a solid-state object as the target, with the surface in the form of a slightly curved trough irradiated under optimal conditions (14) such that its guide lies in the plane of incidence (Fig. 12a). Numerical simulation by the PIC method suggests the possibility or reaching the intensity 1.8×10^{26} W cm^{-2} in a region several nanometers in size using a 10 petawatt laser pulse with the focused intensity 10^{23} W cm^{-2} (Fig. 12b).

5.5 Coherent wakefield radiation

One more popular mechanism to generate higher harmonics is the so-called coherent wakefield radiation [220], which can be described as follows. The interaction between laser radiation and the solid target surface gives rise to electron bunches penetrating deep into the plasma [221]. Given a concentration gradient, the bunches excite plasma oscillations with a frequency that is a multiple of the bunch repetition rate, which in turn depends on the laser pulse frequency. These oscillations occur at a certain concentration gradient and therefore emit electromagnetic waves of the same frequency. As a result, harmonics are generated up to those of the plasma frequency corresponding to the maximum concentration of electrons in the target.

The generation of coherent wakefield radiation was observed in a number of experiments. In 2004, the authors of [222] reported the generation of harmonics at the rear side of targets (thin carbon and aluminum foil) irradiated by a laser with an intensity of the order of 10^{18} W cm^{-2}. The frequency of these harmonics was lower than the target plasma frequency, which suggested that they were generated at the rear edge of the foil by electrons introduced by the laser pulse from the leading edge into the core of the target. In 2006, it was shown, based on numerical computation, that these electrons can just as well generate higher-order harmonics at the leading edge [220]. Characteristically, such generation occurred at subrelativistic intensities. For example, a laser pulse only 2×10^{16} W cm^{-2} in intensity produced harmonics up to the 18th order.

6. Conclusion

Multi-petawatt laser sources that permit reaching intensities of the order of 10^{23} W cm^{-2} may be expected to appear in the near future. Several centers in different countries are simultaneously developing laser systems with the rated peak power up to 10 PW. These are Vulcan-10PW in UK, ILE Apollon in France, and PEARL-10 in Russia. Three super-

power laser facilities are being built in the Czech Republic, Hungary, and Romania in the framework of the European ELI megaproject to provide a basis for research on fundamental physical processes in superstrong electromagnetic fields, the generation of attosecond pulses, and photonuclear processes. The appearance of sources operating at a new power level will allow the practical use of new efficient methods for charged particle accelerators and the generation of radiation with unique characteristics, such as monoenergetic electron beams with energies of several GeV, 1 GeV ion beams, ultrabright gamma radiation with the photon energy of the order of several GeV, ultrashort pulses of subattosecond duration, and attosecond pulses with intensities of the order of 10^{26} W cm^{-2}.

This work was supported by the Russian Academy of Sciences (Presidium of the RAS program "Extreme Light Fields and Their Applications," the DPS RAS program "Non-linear Optical Methods and Materials for Developing a New Generation of Laser Systems"); the Ministry of Science and Education (state contracts 02740.11.0225 and 02.740.11.0563); the Council of the President of Russian Federation for support of young scientists and leading scientific schools (grant NSh-3800.2010.2); and the RFBR grants 09-02-12322-ofi.m and 09-02-12218-ofi.m.

The authors gratefully acknowledge the support (computational resources) of the Joint Supercomputer Center, RAS.

References

1. Strickland D, Mourou G *Opt. Commun.* **56** 219 (1985)
2. Maine P, Mourou G *Opt. Lett.* **13** 467 (1988)
3. Perry M D et al. *Opt. Lett.* **24** 160 (1999)
4. Danson C N et al. *Nucl. Fusion* **44** S239 (2004)
5. Khazanov E A, Sergeev A M *Usp. Fiz. Nauk* **178** 1006 (2008) [*Phys. Usp.* **51** 969 (2008)]
6. Bahk S-W et al. *Opt. Lett.* **29** 2837 (2004)
7. Yanovsky V et al. *Opt. Express* **16** 2109 (2008)
8. Mourou G A, Tajima T, Bulanov S V *Rev. Mod. Phys.* **78** 309 (2006)
9. Norreys P A et al. *Phys. Plasmas* **16** 041002 (2009)
10. Mocker H W, Collins R J *Appl. Phys. Lett.* **7** 270 (1965)
11. Piskarskas A, Stabinis A, Yankauskas A *Usp. Fiz. Nauk* **150** 127 (1986) [*Sov. Phys. Usp.* **29** 869 (1986)]
12. Khazanov E A, Sergeev A M *Laser Phys.* **17** 1398 (2007)
13. Hugonnot E et al. *Appl. Opt.* **46** 8181 (2007)
14. Chekhlov O V et al. *Opt. Lett.* **31** 3665 (2006)
15. Kiriyama H et al. *Opt. Lett.* **32** 2315 (2007)
16. Lozhkarev V V et al. *Laser Phys. Lett.* **4** 421 (2007)
17. Bespalov V I et al. *Izv. Akad. Nauk SSSR. Ser. Fiz.* **51** 1354 (1987)
18. Bespalov V I et al. *Proc. SPIE* **2633** 732 (1995)
19. Litvak A G *Zh. Eksp. Teor. Fiz.* **57** 629 (1968) [*Sov. Phys. JETP* **30** 344 (1969)]
20. Max C E, Arons J, Langdon A B *Phys. Rev. Lett.* **33** 209 (1974)
21. Akhiezer A I, Polovin R V *Zh. Eksp. Teor. Fiz.* **30** 915 (1956) [*Sov. Phys. JETP* **3** 696 (1956)]
22. Kaw P, Dawson J *Phys. Fluids* **13** 472 (1970)
23. Gaponov A V, Miller M A *Zh. Eksp. Teor. Fiz.* **34** 242 (1958) [*Sov. Phys. JETP* **7** 168 (1958)]
24. Kozlov V A, Litvak A G, Suvorov E V *Zh. Eksp. Teor. Fiz.* **76** 148 (1979) [*Sov. Phys. JETP* **49** 75 (1979)]
25. Tajima T, Dawson J M *Phys. Rev. Lett.* **43** 267 (1979)
26. Farina D, Bulanov S V *Phys. Rev. Lett.* **86** 5289 (2001)
27. Teubner U, Gibbon P *Rev. Mod. Phys.* **81** 445 (2009)
28. Belyaev V S et al. *Usp. Fiz. Nauk* **178** 823 (2008) [*Phys. Usp.* **51** 793 (2008)]
29. Joshi C, Malka V *New J. Phys.* **12** 045003 (2010)
30. Esarey E, Schroeder C B, Leemans W P *Rev. Mod. Phys.* **81** 1229 (2009)
31. Krushelnick K, Malka V *Laser Photon. Rev.* **4** 42 (2010)
32. Macchi A *Appl. Phys. B* **82** 337 (2006)
33. Norreys P A et al. *Plasma Phys. Control. Fusion* **40** 175 (1998)
34. Petrov G M, Davis J *Phys. Plasmas* **15** 073109 (2008)
35. Winterfeldt C, Spielmann C, Gerber G *Rev. Mod. Phys.* **80** 117 (2008)
36. Ping Y et al. *Phys. Rev. Lett.* **100** 085004 (2008)
37. Nakatsutsumi M et al. *New J. Phys.* **10** 043046 (2008)
38. Nilson P M et al. *Phys. Rev. E* **79** 016406 (2009)
39. Ichimaru S *Rev. Mod. Phys.* **65** 255 (1993)
40. Labaune C *Nature Phys.* **3** 680 (2007)
41. Tabak M et al. *Phys. Plasmas* **1** 1626 (1994)
42. Tabak M et al. *Phys. Plasmas* **12** 057305 (2005)
43. Esarey E, Sprangle P, Krall J *Phys. Rev. E* **52** 5443 (1995)
44. Plettner T et al. *Phys. Rev. Lett.* **95** 134801 (2005)
45. Kimura W D et al. *Phys. Rev. Lett.* **74** 546 (1995)
46. Sprangle P, Esarey E, Krall J *Phys. Rev. E* **54** 4211 (1996)
47. Gorbunov L M, Kirsanov V I *Zh. Eksp. Teor Fiz.* **93** 509 (1987) [*Sov. Phys. JETP* **93** 509 (1987)]
48. Sprangle P et al. *Appl. Phys. Lett.* **53** 2146 (1988)
49. Rosenbluth M N, Liu C S *Phys. Rev. Lett.* **29** 701 (1972)
50. Joshi C et al. *Nature* **311** 525 (1984)
51. Kitagawa Y et al. *Phys. Rev. Lett.* **68** 48 (1992)
52. Clayton C E et al. *Phys. Rev. Lett.* **70** 37 (1993)
53. Everett M et al. *Nature* **368** 527 (1994)
54. Tang C M, Sprangle P, Sudan R N *Phys. Fluids* **28** 1974 (1985)
55. Horton W, Tajima T *Phys. Rev. A* **34** 4110 (1986)
56. McKinstrie C J, Forslund D W *Phys. Fluids* **30** 904 (1987)
57. Esarey E, Ting A, Sprangle P *Appl. Phys. Lett* **53** 1266 (1988)
58. Gibbon P, Bell A R *Phys. Rev. Lett.* **61** 1599 (1988)
59. Mori W B et al. *Phys. Rev. Lett.* **60** 1298 (1988)
60. Berezhiani V I, Murusidze I G *Phys. Scr.* **45** 87 (1992)
61. Nakajima K *Phys. Rev. A* **45** 1149 (1992)
62. Bonnaud G, Teychenné D, Bobin J-L *Phys. Rev. E* **50** R36 (1994)
63. Dalla S, Lontano M *Phys. Rev. E* **49** R1819 (1994)
64. Umstadter D, Esarey E, Kim J *Phys. Rev. Lett.* **72** 1224 (1994)
65. Andreev N E et al. *Pis'ma Zh. Eksp. Teor. Fiz.* **55** 550 (1992) [*JETP Lett.* **55** 571 (1992)]
66. Antonsen T M (Jr.), Mora P *Phys. Rev. Lett.* **69** 2204 (1992)
67. Sprangle P et al. *Phys. Rev. Lett.* **69** 2200 (1992)
68. Esarey E et al. *Phys. Fluids B* **5** 2690 (1993)
69. Coverdale C A et al. *Phys. Rev. Lett.* **74** 4659 (1995)
70. Modena A et al. *Nature* **377** 606 (1995)
71. Nakajima K et al. *Phys. Rev. Lett.* **74** 4428 (1995)
72. Moore C I et al. *Phys. Rev. Lett.* **79** 3909 (1997)
73. Wagner R et al. *Phys. Rev. Lett.* **78** 3125 (1997)
74. Gordon D et al. *Phys. Rev. Lett.* **80** 2133 (1998)
75. Leemans W P et al. *Phys. Plasmas* **8** 2510 (2001)
76. Leemans W P et al. *Phys. Rev. Lett.* **89** 174802 (2002)
77. Malka V et al. *Phys. Plasmas* **8** 2605 (2001)
78. Chen W-T et al. *Phys. Rev. Lett.* **92** 075003 (2004)
79. Umstadter D et al. *Science* **273** 472 (1996)
80. Ting A et al. *Phys. Plasmas* **4** 1889 (1997)
81. Gahn C et al. *Phys. Rev. Lett.* **83** 4772 (1999)
82. Malka V et al. *Science* **298** 1596 (2002)
83. Kruer W L *The Physics of Laser Plasma Interactions* (Redwood City, Calif.: Addison-Wesley, 1988)
84. Gorbunov L, Mora P, Antonsen T M (Jr.) *Phys. Rev. Lett.* **76** 2495 (1996)
85. Gorbunov L M, Mora P, Antonsen T M (Jr.) *Phys. Plasmas* **4** 4358 (1997)
86. Andreev N E et al. *Phys. Plasmas* **4** 1145 (1997)
87. Schroeder C B et al. *Phys. Plasmas* **13** 033103 (2006)
88. Kalmykov S Yu et al. *Phys. Plasmas* **13** 113102 (2006)
89. Joshi C et al. *Phys. Rev. Lett.* **47** 1285 (1981)
90. Bertrand P et al. *Phys. Plasmas* **2** 3115 (1995)
91. Esarey E et al. *Phys. Rev. Lett.* **80** 5552 (1998)
92. Tzeng K-C, Mori W B, Katsouleas T *Phys. Rev. Lett.* **79** 5258 (1997)
93. Umstadter D et al. *Phys. Rev. E* **51** 3484 (1995)
94. Esarey E et al. *Phys. Rev. Lett.* **79** 2682 (1997)
95. Hemker R G et al. *Phys. Rev. E* **57** 5920 (1998)
96. Schroeder C B et al. *Phys. Rev. E* **59** 6037 (1999)
97. Fubiani G et al. *Phys. Rev. E* **70** 016402 (2004)
98. Kotaki H et al. *Phys. Plasmas* **11** 3296 (2004)

99. Faure J et al. *Nature* **444** 737 (2006)
100. Kotaki H et al. *IEEE Trans. Plasma Sci.* **36** 1760 (2008)
101. Bulanov S et al. *Phys. Rev. E* **58** R5257 (1998)
102. Suk H et al. *Phys. Rev. Lett.* **86** 1011 (2001)
103. Tomassini P et al. *Phys. Rev. ST Accel. Beams* **6** 121301 (2003)
104. Kim J U, Hafz N, Suk H *Phys. Rev. E* **69** 026409 (2004)
105. Chien T-Y et al. *Phys. Rev. Lett.* **94** 115003 (2005)
106. Brantov A V et al. *Phys. Plasmas* **15** 073111 (2008)
107. Geddes C G R et al. *Phys. Rev. Lett.* **100** 215004 (2008)
108. Leemans W P et al. *Nature Phys.* **2** 696 (2006)
109. Nakamura K et al. *Phys. Plasmas* **14** 056708 (2007)
110. Sprangle P, Esarey E, Ting A *Phys. Rev. Lett.* **64** 2011 (1990)
111. Sprangle P, Esarey E, Ting A *Phys. Rev. A* **41** 4463 (1990)
112. Shadwick B A et al. *IEEE Trans. Plasma Sci.* **30** 38 (2002)
113. Esarey E, Pilloff M *Phys. Plasmas* **2** 1432 (1995)
114. Schroeder C B, Esarey E, Shadwick B A *Phys. Rev. E* **72** 055401(R) (2005)
115. Mora P, Antonsen T M (Jr.) *Phys. Rev. E* **53** R2068 (1996)
116. Pukhov A, Meyer-ter-Vehn J *Appl. Phys. B* **74** 355 (2002)
117. Lu W et al. *Phys. Plasmas* **13** 056709 (2006)
118. Faure J et al. *Nature* **431** 541 (2004)
119. Geddes C G R et al. *Nature* **431** 538 (2004)
120. Mangles S P D et al. *Nature* **431** 535 (2004)
121. Kneip S et al. *Phys. Rev. Lett.* **103** 035002 (2009)
122. Kaluza M C et al. *Phys. Rev. Lett.* **105** 115002 (2010)
123. Froula D H et al. *Phys. Rev. Lett.* **103** 215006 (2009)
124. Ralph J E et al. *Phys. Plasmas* **17** 056709 (2010)
125. Soloviev A A et al. *Nucl. Phys. A* (in press)
126. Clayton C E et al. *Phys. Rev. Lett.* **105** 105003 (2010)
127. Krall J et al. *Phys. Rev. E* **48** 2157 (1993)
128. Bulanov S V, Pegoraro F, Pukhov A M *Phys. Rev. Lett.* **74** 710 (1995)
129. Hidding B et al. *Phys. Rev. Lett.* **96** 105004 (2006)
130. Hidding B et al. *Phys. Rev. Lett.* **104** 195002 (2010)
131. Rosenzweig J B et al. *Phys. Rev. A* **44** R6189 (1991)
132. Geindre J P, Marjoribanks R S, Audebert P *Phys. Rev. Lett.* **104** 135001 (2010)
133. Eremin V I, Korzhimanov A V, Kim A V *Phys. Plasmas* **17** 043102 (2010)
134. Sauerbrey R et al. *Phys. Plasmas* **1** 1635 (1994)
135. Cerchez M et al. *Phys. Rev. Lett.* **100** 245001 (2008)
136. Nakatsutsumi M et al. *J. Phys. Conf. Ser.* **112** 022063 (2008)
137. Bula C et al. *Phys. Rev. Lett.* **76** 3116 (1996)
138. Burke D L et al. *Phys. Rev. Lett.* **79** 1626 (1997)
139. Bamber C et al. *Phys. Rev. D* **60** 092004 (1999)
140. Jackson J D *Classical Electrodynamics* (New York: Wiley, 1962) [Translated into Russian (Moscow: Mir, 1965)]
141. Landau L D, Lifshitz E M *Teoriya Polya* (The Classical Theory of Fields) (Moscow: Fizmatlit, 2006) [Translated into English (Oxford: Pergamon Press, 1980)]
142. Hatchett S P et al. *Phys. Plasmas* **7** 2076 (2000)
143. Wilks S C et al. *Phys. Plasmas* **8** 542 (2001)
144. Passoni M, Bertagna L, Zani A *New J. Phys.* **12** 045012 (2010)
145. Hegelich B M et al. *Nature* **439** 441 (2006)
146. Schwoerer H et al. *Nature* **439** 445 (2006)
147. Nodera Y et al. *Phys. Rev. E* **78** 046401 (2008)
148. Takahashi K et al. *Phys. Plasmas* **17** 093102 (2010)
149. Wang F et al. *Phys. Plasmas* **16** 093112 (2009)
150. Pae K H et al. *Phys. Plasmas* **16** 073106 (2009)
151. Esirkepov T et al. *Phys. Rev. Lett.* **92** 175003 (2004)
152. Lebedew P *Ann. Physik* **311** 433 (1901)
153. Macchi A et al. *Phys. Rev. Lett.* **94** 165003 (2005)
154. He F et al. *Phys. Plasmas* **13** 073102 (2006)
155. Yan X Q et al. *Phys. Rev. Lett.* **100** 135003 (2008)
156. Davis J, Petrov G M *Phys. Plasmas* **16** 023105 (2009)
157. He M-Q et al. *Phys. Rev. E* **76** 035402(R) (2007)
158. Holkundkar A R, Gupta N K *Phys. Plasmas* **15** 123104 (2008)
159. Zhang X et al. *Phys. Plasmas* **14** 073101 (2007)
160. Zhang X et al. *Phys. Plasmas* **14** 123108 (2007)
161. Liseikina T V, Macchi A *Appl. Phys. Lett.* **91** 171502 (2007)
162. Macchi A, Veghini S, Pegoraro F *Phys. Rev. Lett.* **103** 085003 (2009)
163. Macchi A et al. *New J. Phys.* **12** 045013 (2010)
164. Pegoraro F, Bulanov S V *Phys. Rev. Lett.* **99** 065002 (2007)
165. Robinson A P L et al. *New J. Phys.* **10** 013021 (2008)
166. Klimo O et al. *Phys. Rev. ST Accel. Beams* **11** 031301 (2008)
167. Pegoraro F, Bulanov S V *Eur. Phys. J. D* **55** 399 (2009)
168. Chen M et al. *Phys. Plasmas* **15** 113103 (2008)
169. Chen M et al. *Phys. Rev. Lett.* **103** 024801 (2009)
170. Yan X Q et al. *Phys. Rev. Lett.* **103** 135001 (2009)
171. Qiao B et al. *Phys. Rev. Lett.* **102** 145002 (2009)
172. Yu T-P et al. *Phys. Rev. Lett.* **105** 065002 (2010)
173. Kar S et al. *Phys. Rev. Lett.* **100** 225004 (2008)
174. Henig A et al. *Phys. Rev. Lett.* **103** 245003 (2009)
175. Doumy G et al. *Phys. Rev. E* **69** 026402 (2004)
176. Korzhimanov A V et al. *Pis'ma Zh. Eksp. Teor. Fiz.* **86** 662 (2007) [*JETP Lett.* **86** 577 (2007)]
177. Korzhimanov A V et al. *Zh. Eksp. Teor. Fiz.* **132** 771 (2007) [*JETP Lett.* **105** 675 (2007)]
178. Gonoskov A A et al. *Phys. Rev. Lett.* **102** 184801 (2009)
179. Shen B et al. *Phys. Rev. E* **76** 055402(R) (2007)
180. Shen B et al. *Phys. Rev. ST Accel. Beams* **12** 121301 (2009)
181. Yin L et al. *Phys. Plasmas* **14** 056706 (2007)
182. Buneman O *Phys. Rev. Lett.* **1** 8 (1958)
183. Albright B J et al. *Phys. Plasmas* **14** 094502 (2007)
184. Agostini P, DiMauro L F *Rep. Prog. Phys.* **67** 813 (2004)
185. Krausz F, Ivanov M *Rev. Mod. Phys.* **81** 163 (2009)
186. Ferray M et al. *J. Phys. B: At. Mol. Opt. Phys.* **21** L31 (1988)
187. Corkum P B *Phys. Rev. Lett.* **71** 1994 (1993)
188. Chang Z et al. *Phys. Rev. Lett.* **79** 2967 (1997)
189. Spielmann Ch et al. *Science* **278** 661 (1997)
190. Goulielmakis E et al. *Science* **320** 1614 (2008)
191. Carman R L, Forslund D W, Kindel J M *Phys. Rev. Lett.* **46** 29 (1981)
192. Bezzerides B, Jones R D, Forslund D W *Phys. Rev. Lett.* **49** 202 (1982)
193. Bulanov S V, Naumova N M, Pegoraro F *Phys. Plasmas* **1** 745 (1994)
194. Lichters R, Meyer-ter-Vehn J, Pukhov A *Phys. Plasmas* **3** 3425 (1996)
195. Gibbon P *Phys. Rev. Lett.* **76** 50 (1996)
196. Zepf M et al. *Phys. Rev. E* **58** R5253 (1998)
197. Tarasevitch A et al. *Phys. Rev. A* **62** 023816 (2000)
198. Gordienko S et al. *Phys. Rev. Lett.* **93** 115002 (2004)
199. Gordienko S et al. *Phys. Rev. Lett.* **94** 103903 (2005)
200. Baeva T, Gordienko S, Pukhov A *Phys. Rev. E* **74** 046404 (2006)
201. Dromey B et al. *Nature Phys.* **2** 456 (2006)
202. Dromey B et al. *Phys. Rev. Lett.* **99** 085001 (2007)
203. Dromey B et al. *Nature Phys.* **5** 146 (2009)
204. Boyd T J M, Ondarza-Rovira R *Phys. Rev. Lett.* **101** 125004 (2008)
205. an der Brügge D, Pukhov A *Phys. Plasmas* **17** 033110 (2010)
206. Hentschel M et al. *Nature* **414** 509 (2001)
207. Plaja L et al. *J. Opt. Soc. Am. B* **15** 1904 (1998)
208. Pirozhkov A S et al. *Phys. Plasmas* **13** 013107 (2006)
209. Tsakiris G D et al. *New J. Phys.* **8** 19 (2006)
210. Geissler M et al. *New J. Phys.* **9** 218 (2007)
211. Naumova N M et al. *Phys. Rev. Lett.* **92** 063902 (2004)
212. Rykovanov S G et al. *New J. Phys.* **10** 025025 (2008)
213. Nomura Y et al. *Nature Phys.* **5** 124 (2009)
214. Fedotov A M et al. *Phys. Rev. Lett.* **105** 080402 (2010)
215. The Extreme Light Infrastructure. European Project, http://www.extreme-light-infrastructure.eu
216. Bulanov S V, Esirkepov T, Tajima T *Phys. Rev. Lett.* **91** 085001 (2003)
217. Kulagin V V et al. *Phys. Rev. Lett.* **99** 124801 (2007)
218. Gonoskov A A et al. *Phys. Rev. Lett.* (in preparation)
219. SimLight Group, http://ipfran.ru/structure/lab334/simlight.html
220. Quéré F et al. *Phys. Rev. Lett.* **96** 125004 (2006)
221. Brunel F *Phys. Rev. Lett.* **59** 52 (1987)
222. Teubner U et al. *Phys. Rev. Lett.* **92** 185001 (2004)